Running head: S-sulfocysteine synthase function in photosynthetic adaptation to photoperiod

Correspondence: Luis C. Romero. Instituto de Bioquímica Vegetal y Fotosíntesis. Consejo Superior de Investigaciones Científicas and Universidad de Sevilla. Avenida Américo Vespucio, 49, 41092 Sevilla, Spain. Tel: 34.954489516. Fax: 34.954460065. E-mail: lromero@ibvf.csic.es

Journal research area:

Photosynthetic adaptation to length of day is dependent on S-sulfocysteine synthase activity in the thylakoid lumen

María Ángeles Bermúdez[1], Jeroni Galmés[2], Inmaculada Moreno[1], Philip M. Mullineaux[3], Cecilia Gotor[1], Luis C. Romero[1*]

[1]Instituto de Bioquímica Vegetal y Fotosíntesis, Consejo Superior de Investigaciones Científicas y Universidad de Sevilla, Avenida Américo Vespucio, 49, 41092 Sevilla, Spain.
[2]Grup de Recerca en Biologia de les Plantes en Condicions Mediterrànies, Universitat de les Illes Balears, 07122 Palma, Spain.
[3]School of Biological Sciences, University of Essex, Colchester CO4 3SQ, United Kingdom.

Footnotes:

This work was funded in part by the European Regional Development Fund (ERDF) through the Ministerio de Ciencia e Innovación (grants no. BIO2010-15201 and AGL2009-07999), the Junta de Andalucía (grant nos. P06-CVI-01737 and BIO–273) and the CONSOLIDER CSD2007–00057 (Spain).

Corresponding author: Luis C. Romero, e-mail: lromero@ibvf.csic.es

ABSTRACT

Arabidopsis thaliana chloroplasts contain two O-acetylserine(thiol)lyase (OASTL) homologues, OAS-B, which is an authentic OASTL, and CS26, which has S-sulfocysteine synthase activity. In contrast with OAS-B, the loss of CS26 function resulted in dramatic phenotypic changes, which were dependent on the light treatment. We have performed a detailed characterisation of the photosynthetic and chlorophyll fluorescence parameters in *cs26* plants compared with those of wild-type under short- (SD) and long-day (LD) growth conditions. Under LD, the photosynthetic characterisation, which was based on C_i- and C_c-curves, revealed significant reductions in most of the photosynthetic parameters for *cs26*, which were unchanged under SD. These parameters included net CO_2 assimilation rate (A_N), mesophyll conductance (g_m) and mitochondrial respiration at darkness (R_{dark}). The analysis also showed that *cs26* under LD required more absorbed quanta per driven electron flux and fixed CO_2. The non-photochemical quenching (NPQ) values suggested that in *cs26* plants, the excess electrons that are not used in photochemical reactions may form ROS. A photoinhibitory effect was confirmed by the F_o values under LD and SD, which were higher in young leaves compared with mature ones under SD. To hypothesise the role of CS26 in relation to the photosynthetic machinery, we addressed its location inside of the chloroplast. The activity determination and localisation analyses that were performed using immunoblotting indicated the presence of an active CS26 enzyme exclusively in the thylakoid lumen. This finding was reinforced by the observation of marked alterations in many lumenal proteins in the *cs26* mutant compared with the wild-type.

INTRODUCTION

In plants, cysteine biosynthesis is accomplished by the sequential reaction of two enzymes, serine acetyltransferase (SAT), which catalyses the synthesis of the intermediary product O-acetylserine (OAS) from acetyl-CoA and serine, and O-acetylserine(thiol)lyase, which incorporates the sulphide that is derived from the assimilatory reduction of sulphate to OAS, producing cysteine. Both enzymes interact to form the hetero-oligomeric cysteine synthase complex, which was first described in bacteria and is now extensively studied in plants (Droux *et al*., 1998; Wirtz and Hell, 2006). Plant cells contain different SAT and OASTL enzymes that are localised to the cytosol, plastids and mitochondria, resulting in a complex variety of isoforms and distinct subcellular cysteine pools. *Arabidopsis thaliana* contains five different *SAT* (Howarth *et al*., 2003) and nine *OASTL* genes (Wirtz *et al*., 2004).

Arabidopsis chloroplasts contain two OASTL homologues that are encoded by the *OAS-B* (At2g43750) and *CS26* (At3g03630) genes. At the transcriptional level, *OAS-B* is the most abundant OASTL transcript, and its encoded protein is considered to be an authentic OASTL because of its ability to interact with SAT (Gilbert *et al*., 1996; Droux *et al*., 1998; Kidner *et al*., 2000; Kim *et al*., 2007). Our group recently investigated *CS26,* clearly demonstrating that the minor chloroplastic OASTL isoform that is encoded by the *CS26* gene from *Arabidopsis* has S-sulfocysteine synthase activity (Bermudez *et al*., 2010); this is the first report of this activity in plants. The CS26 protein is predicted to be localised within the chloroplast on the basis of its N-terminal signal peptide, although this has not yet been demonstrated; however, the predicted amino acid sequence comparison revealed that CS26 contains an extension at the C-terminus of the chloroplast transit peptide in contrast with OAS-B. The biochemical comparison of the *oas-b* and *cs26* null mutants demonstrated that the *cs26* mutation had no effect on OASTL activity levels, whereas the *oas-b* mutant had significantly less OASTL activity (Watanabe *et al*., 2008; Bermudez *et al*., 2010). In addition, the loss of CS26 function resulted in dramatic phenotypic changes, which were dependent on the prevailing light treatment. The *cs26* mutant exhibited reduced chlorophyll concentrations and photosynthetic activity, showing elevated glutathione levels, and accumulated reactive oxygen species under long-day growth conditions. Although the function of CS26 has not yet been established, *CS26* has been identified as one of the target genes of the Long Term Response (LTR) signalling pathway, which is regulated to compensate for the lack of LTR signalling (Pesaresi *et al*., 2009).

During optimal photosynthetic conditions, light energy is harvested and channelled into the two reaction centres of PSI and PSII, which are where charge separation occurs and electrons are passed linearly along the electron transport chain leading to ATP and NADPH production for CO_2 fixation into organic compounds. Under constant moderate light conditions, the efficiency of the energy conversion is high as a result of photochemical reactions. Fluctuations in light intensity, temperature or water availability may contribute to the over-excitation of PSII, and photoprotective mechanisms are subsequently activated to prevent damage that either involve the detoxification of the ROS (Asada, 1999) or the prevention of their formation by the dissipation of excess excited states into heat. The failure to dissipate excitation energy results in the over-reduction of the photosynthetic chain components that direct linear electron flux from water to NADPH (Baker, 2008). A portion of the absorbed light energy is dissipated as heat in the light-harvesting complexes of photosystem II (PSII) through non-photochemical quenching (NPQ) (Horton *et al*., 1996; Muller *et al*., 2001). The additional dissipation of excitation energy is also achieved by photochemical quenching through the reduction of molecular oxygen at photosystem I via the Mehler reaction and photorespiration (Asada, 1999; Douce and Neuburger, 1999), of which both processes produce ROS. In light-stressed plants, the damaged chloroplasts initiate retrograde signalling to the nucleus (Pogson *et al*., 2008) to down-regulate the expression of photosynthetic genes and up-regulate stress defence genes to mitigate oxidative stress (Koussevitzky *et al*., 2007; Mühlenbock *et al*., 2008).

The aims of the present work were to reveal the subcellular localisation of CS26 inside the chloroplast and to characterise the photosynthetic limitations that are due to the *CS26* mutation in *Arabidopsis* under different light treatments.

RESULTS

Leaf Morphology of *cs26* Mutant Was Affected by Light Conditions

When the leaf phenotypic traits of the *cs26* mutant line were compared with those of the wild type, no significant differences were reported under short-day conditions (SD), and similar leaf areas and leaf mass areas (LMA) were observed (Fig. 1). However, when the plants were grown under long-day conditions (LD), both the leaf areas and LMAs were reduced by 26 % in the *cs26* mutant compared with the wild-type, suggesting that the leaves

of *cs26* were thinner and/or less dense. Non-visible changes in leaf morphology were observed in the wild-type when comparing the plants that were grown under the two photoperiods (Fig. 1).

Photosynthetic Parameters Were Reduced in *cs26* Mutant Under Long-Day Conditions Compared with Wild-Type

At saturating light conditions and ambient CO_2 concentrations, non-significant differences (P<0.05) were observed between the *cs26* mutant and wild-type under SD for most of the photosynthetic parameters, including net CO_2 assimilation rate (A_N), stomatal conductance (g_s), photosynthetic water-use efficiency (A_N/g_s), mesophyll conductance (g_m), mitochondrial respiration at darkness (R_{dark}) and g_s at darkness ($g_{s,dark}$) (Table I). Under LD, A_N was more severely reduced in the *cs26* mutant (from 8.3 to 1.9 μmol m^{-2} s^{-1}) than in the wild type (from 11.6 to 8.3 μmol m^{-2} s^{-1}). However, the g_s values did not significantly differ when comparing plants that were grown under SD and LD for any of the two genotypes. As a result, A_N/g_s was lower under LD than SD in both lines, but stronger photoperiod effects were observed in *cs26* (Table I). The capacities of the leaf mesophyll to transfer CO_2 from the substomatal cavities to the sites of carboxylation (g_m) were similar between the two lines under SD, but under LD, g_m was severely depressed in *cs26,* while it was stimulated in the wild-type. All of these factors affected the CO_2 concentration in the chloroplast (C_c), leading to higher values in both lines for the plants that were grown under the LD compared with the SD photoperiod. Under SD, no significant differences were observed between the lines with regard to the R_{dark} and $g_{s,dark}$ values, but under LD, the *cs26* mutant showed increased R_{dark} compared with the wild-type (Table I).

Under SD conditions, the parameters that were derived from the A_N-C_i curves were similar between the wild-type and *cs26* (Fig. 2A). However, when the two lines were grown under LD conditions, *cs26* presented lower A_N values for any given C_i, a lower initial slope and a higher CO_2 compensation point on a C_i basis (Fig. 2B). When the A_N-C_i curves were transformed into A_N-C_c curves, a unique difference was revealed between the genotypes under SD; the initial slope ($V_{c,max}$) was significantly lower in *cs26* as a result of the slightly lower g_m values in the wild-type (Table I and Fig. 2C). Under LD conditions, the differences in the A_N-C_i curves were maintained, with a lower $V_{c,max}$ (37 %) and higher CO_2 compensation point on a C_i basis (Γ_{Cc}) (133 %) for *cs26* compared with wild-type (Table I and Fig. 2D). J_{max} was less affected, yet it was 65 % larger in the wild-type under LD and

showed no differences under SD conditions. However, the $J_{max}/V_{c,max}$ ratio stayed almost constant, being slightly higher for the *cs26*-SD plants because of the lower $V_{c,max}$ value for *cs26* under this condition (Table I).

The decrease in $V_{c,max}$ may be due to the lower concentration and/or activation of Rubisco. Under the SD photoperiod, no significant differences in the concentrations of Rubisco and total soluble protein (TSP) were observed between genotypes, but under LD, the *cs26* plants presented 30 % of the Rubisco concentration that was observed in the wild-type (Table II). Remarkably, such a decrease in Rubisco concentration under LD was not completely driven by a decrease in the concentration of total soluble protein (TSP); the ratio Rubisco/TSP was 63 % lower in *cs26* than that of the wild-type.

The response of A_N and the rate of linear electron transport (J) to increasing light intensities differed between the lines when they were grown under LD conditions, with *cs26* showing lower values for any given PAR intensity (Fig. 3A and 3B). At full light-saturating intensities, the corrected J averaged 48.1 and 12.9 μmol e^- m^{-2} s^{-1} for the wild-type and *cs26* line, respectively (Table III). The light intensity at which the A_N-PAR curve showed the inflexion point for *cs26* was nearly half of that of the wild-type because of the presence of lower A_N values. Significant differences between the two lines were also observed for the light compensation point (ca. 3-fold in *cs26*), light use efficiency, as determined from the inverse of the quantum yield (45% higher in *cs26*), and PAR_{abs}/J (ca. 2-fold in *cs26*), indicating that the *cs26* line required more absorbed quanta per driven electron flux and fixed CO_2 (Table III). As expected, under these conditions, the A_N values were similar to those that were obtained from the A_N-C_i curves at a C_a of 400 μmol mol^{-1}; therefore, the *cs26* plants were less efficient at converting electrons into assimilated CO_2 molecules (i.e., lower J/A_G ratios). In fact, at full saturating light, the J/A_G ratio for the mutant was 45 % higher than that for the wild-type (Table III). A closer inspection revealed that at the growth light intensity (approximately 100 μmol m^{-2} s^{-1}), J/A_G displayed the maximum difference between *cs26* and the wild-type (ca. 3.4-fold in *cs26*). The average values for non-photochemical quenching (NPQ) at full-light saturation were also statistically different (ca. 2-fold in *cs26*) (Table III).

Chlorophyll Fluorescence Parameters Showed Differences in *cs26* Plants Compared with Wild-Type, Depending on Light Intensity and Growth Stage

In the wild-type leaves, the maximum quantum efficiency of PSII photochemistry (F_v/F_m) was approximately 0.8 for the plants that had been grown under both SD and LD conditions (Fig. 4A and 4B). In contrast, a reduction in F_v/F_m was observed in the *cs26* leaves that had been grown under both photoperiods compared with those of the wild-type with stronger reductions under LD, indicating a severe defect in PSII. Under SD, the younger rosette leaves from *cs26* presented lower F_v/F_m values when compared with the mature leaves (Fig. 4A). A comprehensive analysis of F_o confirmed that the *cs26* mutant experienced PSII photoinhibition as shown by the high levels of F_o under LD (52 ± 11 in *cs26* compared with 11 ± 1 in wild type). This high value is indicative of lower concentrations of coupled chlorophylls and/or damage to the photosynthetic apparatus. Moreover, the overall F_o value of the *cs26* plants under SD was also higher (62 ± 5 in *cs26* compared with 31 ± 1 in wild type); however, an increase was also observed in F_o in the young leaves compared with the mature ones (89 ± 2 vs. 58 ± 8), verifying the presence of higher photoinhibition in the younger leaves. Under LD, it was also observed that the level of minimal chlorophyll fluorescence from light-adapted leaves (F'_o) was actually reduced by 38 % ($F'_{o,cs26}$= 32 ± 3) compared with F_o in the *cs26* plants, which is unusual. At growth light intensities, *cs*26 showed higher NPQ values under both photoperiods compared with wild-type (Fig. 4C, 4D). Following exposure to 800 μmol m^{-2} s^{-1}, the NPQ increased in both genotypes, indicating the presence of increased heat dissipation from PSII (Fig. 4E, 4F). In mutant plants under SD, the NPQ values were lower in the younger leaves compared with the mature ones irrespective of the actinic light intensity (Fig. 4C, 4E). These data correlate with the F_v/F_m values, suggesting that *cs26* has an important effect at early stages of plant and leaf development. These results are in agreement with the expression of the *CS26* gene in different tissues and developmental stages of *Arabidopsis*, showing the highest transcript accumulation in the leaves of early stage plants (stage 1.07) and stems and flowers (stage 6.1, 10 % of flowers to be produced are opened) (Fig. 5). The accumulation of the *CS26* transcript decreased during the mature stages, showing the lowest values in the leaves of senescent plants (stage 8.0).

Under all of the studied conditions, the *cs26* plants presented lower values for the PSII operating efficiency (F_q'/F_m') compared with the wild-type (Table IV). Similarly, there was a reduction in the maximum efficiency of PSII photochemistry (F_v'/F_m') in the mutant line compared with the wild-type (Table IV). These decreases were independent of the photoperiod or the intensity of the actinic light applied, indicating that the PSII reaction centres were probably damaged because the PSII operating and maximum efficiencies for

the reduction of Q_A were low even under non-saturating light intensities. Consequently, in all cases with the exception of *cs26* under LD at 150 μmol m^{-2} s^{-1}, the PSII efficiency factor (*qP*) was lower in *cs26* than in the wild-type plants.

CS26 Protein Location in Chloroplast Fractions

Comparisons of the deduced amino acid sequences of the homologous OASTL proteins that were located in the chloroplasts revealed that CS26 contains a C-terminal extension to the chloroplast transit peptide in contrast with the other chloroplast OASTL isoform, OAS-B, suggesting that it may be localised to the thylakoid lumen (Bermudez *et al*. 2010). To confirm this observation, we performed a protein blot analysis of the stromal and thylakoid lumenal fractions using anti-CS26 antibodies that were obtained from purified recombinant proteins. Because of the high sequence homologies of the different OASTLs, anti-CS26 antibodies cross-react and recognise other isoforms, including OAS-B; therefore, for an accurate identification, we performed the protein blot analysis in the wild-type and *oas-b* and *cs26* mutant lines.

Representative images of the stained gel and the protein blot analysis are shown in Figure 6. Some Coomassie-stained bands from the stromal and lumenal fractions were excised and analysed by MALDI-TOF, and the detected proteins were identified as the stromal and lumenal proteins, respectively, confirming the high purities of the extracts and validating our results (Fig. 6A and 6C). In addition, a protein blot analysis was also performed using anti-stromal Rubisco activase and anti-lumenal PsbO antibodies to detect any cross-contamination between the stromal and lumenal fractions (Supplemental Fig. S1), again confirming the high purities of the protein extracts.

In the stromal fraction, the anti-CS26 antibodies recognised different proteins, some of which were found in the three lines and had molecular masses of over 45 kDa; hence, they were considered to be non-specific. However, a strong band below 37 kDa was observed in the wild-type and *cs26* that was missing in the *oas-b* mutant (Fig. 6B). The experimental mass of this band was 35.5 kDa and matched the estimated mass of the mature OAS-B protein (35.4 kDa), which may have been due to a cross-reaction with the antibody. Furthermore, in this fraction, a minor band of 40 kDa was observed that was missing in the *cs26* line and matched with the predicted size of the premature CS26 enzyme, which still contains the lumen-targeting transit peptide.

In the lumenal fraction, two bands of different intensities were found in the wild-type

and *oas-b*, but not in *cs26*, that may correspond with the protein CS26 (Fig. 6D). The higher intensity band was found at 34.8 kDa, matching the predictive CS26 mature protein that was calculated by the TargetP and ChloroP programs (www.cbs.dtu.dk) with a mass of 34.1 kDa due to the loss of the lumen-targeting transit peptide. The additional minor band at 40 kDa that was detected in the stromal fractions of the wild-type and *oas-b* lines was also observed in the lumenal fraction and may match with a non-mature form of the CS26 protein without the chloroplast-targeting transit peptide, or it may be the result of post-translational modifications of the protein.

S-sulfocysteine synthase (SSCS) activity was also determined in stromal and lumenal extracts from the wild-type, *oas-b* and *cs26* plants that were grown under LD and SD photoperiods (Fig. 7). Similar results with regard to order of magnitude were obtained in the wild-type and *oas-b* plants, and no activity was detected in the *cs26* plants under either photoperiod. The SSCS activity levels in the stromal fractions were very low compared with the levels that were obtained from the lumenal fractions, which were three orders of magnitude greater. These data suggest that the lumenal-localised CS26 protein of 34.8 kDa is the active form.

Loss of CS26 Protein Strongly Affects Protein Content of Thylakoid Lumen

To further characterise the impact of the loss of CS26 on the chloroplast under LD conditions, we performed a proteome analysis of the thylakoid lumen of LD-grown *cs26* mutant and wild-type plants to determine whether there were significant changes at the protein level in this compartment in the absence of the CS26 protein. The resulting 2-D maps of the lumenal wild-type proteins were highly reproducible and showed very similar protein patterns compared with those that have been previously reported (Kieselbach *et al*., 1998) (Supplemental Fig S2.). Further, almost all of the analysed proteins in the lumenal fraction were identified as lumen-localised (Table V), providing additional validation regarding the purities of the preparations. There were significant differences in the intensities and quantities of the detected proteins in both maps. Despite our strong efforts, we were unable to identify the CS26 protein in the wild-type lumenal fraction. However, we did observe strong alterations in many lumenal proteins of the *cs26* mutant compared with the wild-type. The extrinsic subunits of photosystem II, the PsbP domain protein, HCF136 protein, cyclophilin and FKBP-type peptidyl-prolylcis-trasisomerase, Deg1 and D1-processing proteases, and the peripheral thylakoid ATP synthase CF1 α and β subunits were

all markedly reduced in the null *cs26* mutant, whereas the plastid-lipid-associated protein FBR2 in the thylakoid membrane and plastoglobule was strongly induced in the mutant (Table V). These results suggest that the lack of CS26 protein in the thylakoid lumen greatly affects the stability of many lumenal proteins.

DISCUSSION

Prior to this work, our group established that the phenotypic characteristics of *cs26* mutant plants are dependent on the light treatment. While under short day conditions, *cs26* mutant plants were phenotypically indistinguishable from wild-type plants, when they were grown under long-day conditions, the *cs26* mutant plants exhibited reductions in size and green paleness, and these phenotypic traits were even more severe under continuous light, suggesting a possible defect in photosynthesis under long-day conditions (Bermudez *et al*., 2010). This finding has been confirmed by the present study.

Under LD conditions, the photosynthetic characterisation that was based on the C_i- and C_c-curves revealed significant reductions in most of the photosynthetic parameters in *cs26*, which were restored under the SD photoperiod (Fig. 2 and Table I). Among these parameters, the *cs26* mutants under LD displayed reduced photosynthetic capacities, although they maintained open stomata, resulting in lower photosynthetic water-use efficiencies. In fact, the lower A_N values in *cs26* under LD were due to biochemical limitations (i.e., decreased $V_{c,max}$) and, particularly, a mesophyll conductance limitation (ca. 65% of A_N limitation). The lower $V_{c,max}$ was partially explained by decreased concentrations of Rubisco (Table II). However, we cannot exclude the possibility that part of the reduction in $V_{c,max}$ was due to lower Rubisco activity through an alteration in the redox regulation of Rubisco activase, which is necessary for the light modulation of Rubisco (Zhang *et al*., 2002). It has been shown that g_m depends on leaf morphological characteristics, displaying an inverse correlation with LMA (Flexas *et al*., 2007a). However, this was not the case in the present study, in which decreases in both g_m and LMA were observed (Fig. 1). In other mutant lines with altered redox regulation, increased LMA was observed in LD- compared with SD-grown plants (Lepistö *et al*., 2009).

Remarkably, the photosynthetic performances of wild-type plants were also affected by the photoperiod under which they were grown but to lesser degrees than in the *cs26*

mutants (Table I). Some previous reports have estimated the g_m for *A. thaliana* that is grown under a 12 h light/12 h dark photoperiod to be 250 μmol m^{-2} s^{-1}, although g_m values depend upon plant ontogeny (Flexas *et al*., 2007a). Here, we obtained similar values in the wild-type plants under SD but higher values under LD conditions. Changes in the g_m following the alteration of the spectral quality of light have previously been reported (Loreto *et al*., 2009), but this is the first report of a significant influence of photoperiod length on the regulation of CO_2 transfer through the leaf mesophyll. The increased g_m in LD wild-type plants did not correlate with changes in LMA, suggesting an up-regulation of biochemical factors that are probably related to carbonic anhydrase or aquaporin functioning. To our knowledge, there are no studies available on the regulation of these proteins corresponding with different photoperiod lengths; however, there is evidence that increasing light intensity also increases aquaporin and carbonic anhydrase activities (Moskvin *et al*., 2000; Kim and Steudle, 2007).

Further effects of photoperiod length on the leaf carbon balance were observed in both genotypes (Table I). The increased R_{dark} in LD-grown plants is not related to an increased growth demand for energy because the plants of both genotypes grew less under the LD compared with the SD photoperiod (Bermudez *et al*., 2010). Differences between the respiration rates in LD- and SD-grown wild-type plants may be related to the nature of the substrate that supports the respiration, and additionally, light-enhanced dark respiration has been demonstrated in several plant systems (Reddy *et al*., 1991; Ekelund, 2000; Padmasree *et al*., 2002). In wild-type plants under LD conditions, carbohydrates are used primarily as respiratory substrates, but under SD, there is a shift at the end of a long night from carbohydrates to organic acids due to the limited carbon supply from the starch reserves (Zell *et al*., 2010). Increased dark respiration may also protect photosynthesis from photoinhibition and allow for the dissipation of redox equivalents out of chloroplasts (Saradadevi and Raghavendra, 1992; Singh *et al*., 1996; Raghavendra and Padmasree, 2003).

The analysis of the response of A_N and J to increasing light intensities revealed that *cs26* plants under LD absorbed less light than the wild-type plants (Fig. 3 and Table III). Additionally, there were lower proportions of absorbed photons being converted to electrons and lower amounts of electrons participating in the carboxylation reaction. The fact that NPQ was not particularly activated in the *cs26* plants under non-saturating light conditions (Figure 4C, 4D) suggests that the excess electrons that were not used in photochemical reactions may have developed into reactive oxygen species (ROS). In support of this, an increase in the production of ROS was detected by the histochemical analysis, including the

superoxide radical anion and hydrogen peroxide, in the *cs26* mutant plants under LD conditions (Bermudez *et al*., 2010). R_{dark} showed a greater increase in the LD-grown *cs26* plants, and the transcriptomic data showed a 5.56-fold increase in the mRNA accumulation of a mitochondrial alternative oxidase (AOX) (Gene Expression Omnibus repository GSE19241). AOX can be induced to decrease the level of ROS, but it is clearly insufficient because *cs26* shows severe growth inhibition in LD {Bermudez, 2010 #1852;Yoshida, 2008 #4691}.

A photoinhibition effect was confirmed in the *cs26* mutant according to the F_o values. Additionally, the level of chlorophyll fluorescence before the saturating pulse (F_o') was found to be unusually lower than F_o in the *cs26* plants. Some previous works showed mutants whose fluorescence levels transiently dropped below the F_o level during illumination, similar to the *cs26* mutant. This phenomenon was recently observed in *psbO-1* and *lto1* mutants and mutants of the cytochrome b559 subunit of PSII (Murakami *et al*., 2002; Bondarava *et al*., 2010; Karamoko *et al*., 2011). It has been proposed that the PSII pool is partially reduced in the dark in mutants with low PSII activity, which would result in increased F_o levels, suggesting that the cyclic electron flow pathway would have been activated. Thus, it would allow for the mutants to use PSI and cytochrome b6f to pump protons, thereby synthesising ATP in the absence of significant levels of linear electron flow as a result of the PSII deficiency.

The lack of *CS26* and photosynthetic defects seem to be associated with developmental stages of growth under SD conditions. Data that were obtained from the *cs26* mutant showed opposite trends with regard to the normal evolution of photosynthetic efficiency during wild-type leaf development (Stessman *et al*., 2002) and correlated with an accumulation of the *CS26* transcript in earlier stages (Fig. 5). Therefore, the loss of *CS26* seems to have a significant impact in early developmental stages.

The dramatic effect of the loss of function of the CS26 protein in the chloroplast suggests that S-sulfocysteine synthase enzyme activity or the metabolite S-sulfocysteine play critical roles in maintaining the photosynthetic machinery. To make a hypothesis regarding the function of this enzyme, it is essential to confirm the subcellular localisation of this protein. Prior to this work, a comparison of the amino acid-deduced sequences of several OASTL proteins revealed that CS26 contains an extension at the C-terminus of the chloroplast transit peptide (cTP) in contrast with OAS-B. Using the ChlorP and TargetP cellular localisation programs, the cleavage site predictions of OAS-B and CS26 indicated transit peptide lengths of 58 and 84 amino acids, respectively, which correlate with average-

sized chloroplast transit peptides (cTP) and the total presequence of lumenal proteins (cTP + ITP). Lumen-targeting proteins codified by the nuclear genome are synthesised in the cytosol by a bipartite N-terminal peptide transit with two signals in tandem that share a similar structure with prokaryotic sequences that use the Sec/Tat systems (Robinson *et al*., 2001; Gutensohn *et al*., 2006; Aldridge *et al*., 2009). The transit peptides are characterised by an N-terminal basic region, a hydrophobic central core and a polar C-terminal region ending in an Ala-X-Ala terminal processing site. Proteins that are destined to be transported by the Tat pathway contain a characteristic pair of arginine residues in the N-terminal region of the signal peptide (Aldridge *et al*., 2009). The extension of the lumen-targeting transit peptide of CS26 is compatible with this structure, possessing a basic N-terminal domain with 6 Lys and 1 Arg, a hydrophobic central domain with 6 Pro residues and a polar C-terminal domain with some Asp residues. Although the lumen transit peptide of CS26 does not have the Ala-X-Ala processing site or the ArgArg residues that are necessary for the Tat transport system, it does possess the LysArg modification that has been described for some proteins that use the Tat system (Peltier *et al*., 2002).

Massive proteomic analyses did not allow for the identification of the CS26 protein in any previous work, suggesting that it is present at low levels (Zybailov *et al*., 2008). Activity determination and localisation analyses by protein blot supported the idea of the predicted subcellular localisation of CS26, showing the presence of the enzyme in both the stromal and lumenal fractions, but it was much more abundant in the latter compartment (Fig. 6). However, its activity was almost exclusive to the thylakoid lumen (Fig. 7), with residual activity in the stromal fraction that may be due to some undetected thylakoid contamination. Nevertheless, the pre-processed enzyme may be partially active in the stroma. This analysis also revealed that the OAS-B protein is localised specifically to the chloroplastic stroma.

The comparison of the profiles of the proteins in the thylakoid lumen by 2-D electrophoresis for wild-type and *cs26* allowed for the identification of different proteins that dramatically decrease in abundance in the absence of CS26 in this compartment (Table V). For example, the peripheral thylakoid ATP synthase CF1 α and β subunits were strongly reduced in the *cs26* mutant. This defect was also observed in the *flu* mutant, showing high accumulations of ROS that significantly affected ATP synthase activity (Mahler *et al*., 2007). Furthermore, the HCF136 and Deg1 protein levels were very low in the *cs26* mutant, which are essential for the correct assembly and repair of PSII (Meurer *et al*., 1998; Kapri-Pardes *et al*., 2007). HCF136 has been described in cyanobacteria and plants as an essential

protein for the biogenesis and assembly of PSII because of its stabilization of the newly synthesised D1 protein and its subsequent binding to a D2-cytochrome b559 pre-complex (Plücken *et al*., 2002; Komenda *et al*., 2008). Similarly, Deg1 is involved in photoinhibition repair by degrading the PSII reaction centre protein D1 (Kapri-Pardes *et al*., 2007). PSII repair is known to involve the partial disassembly of PSII, degradation of the damaged proteins, and incorporation and reassembly of the newly synthesised proteins (Nixon *et al*., 2010). Therefore, the reduction of HCF136 and Deg1 and other proteins, such as TLP38 and FKBP-type proteins that are involved in the correct folding of lumenal proteins, may strongly affect the assembly and repair of the photosynthetic machinery and therefore photosynthetic performance.

The comparative wild-type vs. *cs26* lumenal proteomic analysis revealed only one significantly up-regulated protein in *cs26*. This protein is FIBRILLIN 2, which belongs to the PAP/fibrilline-like family that is localised to the plastoglobules (Vidi *et al*., 2006; Lundquist *et al*., 2012). Curiously, it has been described that the numbers of plastoglobules increase in plants that are subjected to environmental conditions that produce oxidative stress on the photosynthetic apparatus (Sam *et al*., 2003; Munn *et al*., 2004).

The mutant phenotype and the photosynthetic rates that are observed in *cs26* under LD but not SD conditions are indicative of severe damage to the photosynthetic machinery by failure of the repair mechanisms of the photosystems during periods of prolonged exposure to light. In conclusion, when grown under low light intensity during long photoperiod the *cs26* mutant behaves as it would be exposed to high irradiance.

As previously mentioned, a similar phenotype has been recently described in a null mutant of the *LTO1* gene that encodes for a lumen thioloxidoreductase that catalyses the formation of disulphide bonds in the thylakoid lumen (Karamoko *et al*., 2011). This enzyme is required for the assembly of PSII through the formation of disulphide bonds in the PsbO subunit of the lumenal PSII oxygen-evolving complex (Karamoko *et al*., 2011). The metabolite S-sulfocysteine, which is synthesised inside of the lumen by CS26, may function in a similar manner by up-regulating the oxidation of the Cys residues of lumenal proteins whose activities are modified by these oxidation events (Buchanan and Luan, 2005), such as FKBP13, which interacts with the Rieske protein (Gopalan *et al*., 2004). Other target lumenal proteins of S-sulfocysteine include STN7 kinase, which is involved in LHCII, and CP29, which is phosphorylated during photosynthetic acclimation and the high light-induced disassembly of PSII complexes, respectively (Pesaresi *et al*., 2009; Fristedt and Vener, 2011). Since S-Cys may act chemically as an oxidative molecule by reacting with reduced

thiols (Neta and Huie, 1985), the absence of the S-sulfocysteine synthase enzyme in the lumen may alter the redox regulation of proteins that are essential for maintaining the repair mechanisms of the photosystems, thereby causing plant light sensitivity in certain lighting conditions.

In conclusion, our studies suggest that the protein CS26, which is located in the thylakoid lumen, is essential for the proper photosynthetic performance of Arabidopsis chloroplasts, and consequently, the loss of CS26 has a dramatic impact on photosynthetic parameters, particularly under long-day growth conditions.

MATERIALS AND METHODS

Plant Materials and Growth Conditions

The *Arabidopsis thaliana* wild-type ecotype Col-0 and the SALK_034133 (*cs26*) and GABI_684B07 (*oas-b*) T-DNA insertion mutant lines were used in this work (Bermudez *et al*., 2010). The plants were grown in soil under a long-day photoperiod (LD) of 16 h of white light (120 µmol m^{-2} s^{-1}) at 22 ºC/8 h of dark at 20 ºC for 3 weeks, or under a short-day photoperiod (SD) of 8 h of white light (same intensity as above) at 22 ºC/16 h of dark at 20 ºC for 5 weeks.

Leaf Mass Area

Leaf mass areas (LMA) were measured for five fully expanded leaves from different individuals per line and calculated as the ratios of leaf dry weights to leaf areas. Dry weights were determined after oven drying for 48 h at 60°C.

Gas Exchange and Chlorophyll Fluorescence Measurements

Leaf gas exchange and chlorophyll a fluorescence were measured simultaneously with an open infrared gas-exchange analyser system that was equipped with a leaf chamber fluorometer (Li-6400-40, Li-Cor Inc., Nebraska, USA). Environmental conditions in the leaf chamber consisted of a leaf-to-air vapour pressure deficit of 1.2-1.8 kPa and a leaf temperature of 22 ºC. The amount of blue light was set to 10 % PPFD to maximise stomatal aperture. Gas exchange and chlorophyll fluorescence measurements included determinations of the net CO_2 assimilation rate and fluorescence parameters at varying photosynthetic active radiation intensities (A_N–PAR curves) and substomatal CO_2 concentrations (A_N-C_i curves). Six A_N-PAR curves per line were obtained from different plants that were grown

under the LD photoperiod. The CO_2 concentration (C_a) within the leaf chamber was maintained at 400 µmol CO_2 mol^{-1} air. In the dark-adapted leaves, measurements were initiated at a photosynthetic photon flux density (PPFD) of zero to obtain values for dark respiration (R_{dark}), dark stomatal conductance ($g_{s,dark}$) and the maximum quantum efficiency of PSII (F_v/F_m). For F_v/F_m, a measuring light of 0.5 µmol photon m^{-2} s^{-1} was set at a frequency of 600 Hz to determine the background fluorescence signal (F_o). To obtain the maximum fluorescence (F_m), saturation pulses of 8500 µmol photon m^{-2} s^{-1} for 0.8 s were applied. F_v/F_m was calculated as $F_v/F_m = (F_m-F_o)/F_m$. Thereafter, gas exchange and chlorophyll fluorescence were measured at increasing PAR intensities up to 2000 µmol m^{-2} s^{-1}, with a total of twelve different intensities.

The actual quantum efficiency of photosystem II (PSII)-driven electron transport was determined according to Genty *et al*. (1989) as:

$$\phi_{PSII} = (F_m' - F_s')/F_m'$$

where F_s' is the steady-state fluorescence of the light (PPFD 1000 µmol m^{-2} s^{-1}), and F_m' is the maximum fluorescence in the light, which was obtained using a light-saturating pulse (8500 µmol m^{-2} s^{-1}) (Genty *et al*., 1989). Because ϕ_{PSII} represents the number of electrons that are transferred per photon absorbed by PSII, the rate of electron transport (J) was calculated as:

$$J = \phi_{PSII} \cdot \text{PPFD} \cdot \alpha \cdot \beta$$

where α is the leaf absorbance, and β is the distribution of absorbed energy between the two photosystems. The product $\alpha \cdot \beta$ was determined from the relationship between ϕ_{PSII} and the quantum efficiency of photosynthesis ($\phi CO_2 = A_N + R_L$ / PPFD), which was obtained by varying the light intensity under non-photorespiratory conditions in an atmosphere containing ca. 1 % O_2 (Warren and Dreyer, 2006) in the wild-type and *cs26* mutant lines under the two photoperiods. The rate of non-photorespiratory CO_2 evolution in the light (R_L) was assumed to be half of R_{dark} (Galmés *et al*., 2011). The product of $\alpha \cdot \beta$ was 0.365 ± 0.007 and 0.470 ± 0.013 for wild-type under LD and SD conditions, respectively, whereas it was 0.267 ± 0.015 and 0.419 ± 0.019 for the *cs26* mutant under LD and SD conditions, respectively.

Six A_N–C_i curves per line were obtained from different plants for each photoperiod. In the light adapted leaves, photosynthesis was initiated at a C_a of 400 µmol mol^{-1} and a saturating PPFD of 1000 µmol m^{-2} s^{-1} (the light saturation that was assessed by light response curves was near 800 µmol m^{-2} s^{-1}). Once steady state was reached (typically after 20 min), C_a was decreased stepwise down to 50 µmol mol^{-1} air. Upon completion of the

measurements at low C_a, it was returned to 400 µmol mol^{-1} air to restore the original A_N. Next, C_a was increased stepwise to 2000 µmol mol^{-1} air. The A_N–C_i curves consisted of eleven different C_a values and were transformed to A_N–C_c curves as described below.

Mesophyll conductance (g_m) was estimated following the variable *J* method (Harley *et al*., 1992) as:

$$g_m = A_N/(C_i-(\Gamma^*(J+8(A_N+R_L)))/(J-4(A_N+R_L)))$$

The Rubisco specificity factor ($S_{C/O}$) has not yet been published for *Arabidopsis thaliana*, and hence, the chloroplast CO_2 compensation point (Γ*) was obtained as a proxy of the substomatal CO_2 compensation point in the absence of mitochondrial respiration (C_i*), which was estimated according to the method of Laisk as described (Galmes *et al*., 2006). Because values for $S_{C/O}$, and hence Γ*, depend upon the amino acid compositions of Rubisco subunits, they do not differ between lines of the same species. Therefore, only wild-type plants were used to estimate Γ*. At 22ºC, a C_i* value of 41.2 ± 2.6 mmol CO_2 mol^{-1} air was obtained (n = 4). Applying the temperature dependence functions that were described by Bernacchi (Bernacchi *et al*., 2002) resulted in a C_i* of 48.4 ± 2.6 at 25ºC, which was similar to previously reported values (Flexas *et al*., 2007a).

Estimated g_m values were used to convert the A_N–C_i curves into A_N–C_c curves. The maximum velocity of carboxylation ($V_{c,max}$) and maximum capacity for electron transport rate (J_{max}) were then calculated from the A_N–C_c curves (Flexas *et al*., 2007a). With the exception of Γ*, the kinetic parameters of Rubisco and its temperature dependence were taken from a previous report (Bernacchi *et al*., 2001)

Corrections for the leakage of CO_2 into and out of the leaf chamber of the Li-6400 were applied to all gas-exchange data (Flexas *et al*., 2007c).

Chlorophyll Fluorescence Imaging

Chlorophyll fluorescence parameters were measured using a FlourImager chlorophyll fluorescent imaging system (Technologica Ltd, Essex, UK). The method applied involved pre-programmed treatments of 30 min dark periods to determine F_v/F_m, for which F_m was obtained at saturation pulses of approximately 5600 µmol photon m^{-2} s^{-1}. Actinic growth light (150 µmol m^{-2} s^{-1}) and saturating light (800 µmol m^{-2} s^{-1}) exposure times and saturating light pulses were applied to obtain the following parameters: F_v/F_m, ϕ_{PSII}, PSII maximum efficiency (F_v'/F_m', where F_v' is equal to $F_m–F_o'$, and F_o' is the minimal fluorescence level of light at which Q_A is maximally oxidised), non-photochemical quenching (*NPQ*, which is calculated from (F_m/F_m') – 1) and PSII efficiency factor (*qP* or

F_q'/F_v'). Three values at each actinic light intensity for 3 replicates per line were obtained for both photoperiods. The calculations and imaging of the parameters were performed automatically using the FluorImager software. *qL* was calculated post-measurements from the images of F_q'/F_m', F_o', and F_s', given by $(F_q'/F_m')/(F_o'/F_s')$ (Baker, 2008).

Quantification of Rubisco Protein

Leaves from plants that were grown under both photoperiods were ground in 50 mM TRIS-HCl (pH 7.5), the extract was centrifuged at 7500 x *g* for 15 min, and the total soluble protein level was determined in the supernatant according to the method of Bradford (Bradford, 1976). The protein aliquots (5 µg) and pure Rubisco were subject to SDS-PAGE using 12 % (w/v) polyacrylamide gels and Coomassie Brilliant Blue staining. The Rubisco titration was performed by quantification with the Quantity One software (Bio-Rad, California, USA) using known concentrations of purified Rubisco from *Arabidopsis thaliana*.

RNA Isolation and *CS26* Expression by Real-Time RT-PCR Analysis

The RNA isolation and real-time PCR analysis of the expression of the *CS26* gene were performed at different stages of development in the wild-type plants, according to the growth stages that were described by Boyes (Boyes *et al*., 2001). At each developmental stage, total RNA from the rosette leaves and stems and flowers at the developmental stage 6.1 were extracted and analysed. Real-time RT-PCR analyses were performed as previously described (Bermudez *et al*., 2010).

Assay of Enzymatic Activity

S-sulfocysteine synthase (SSCS) activity was measured as described previously (Bermudez *et al*., 2010).

Isolation of Stromal and Thylakoid Lumenal Contents and Immunoblot Analyses

Enriched chloroplast preparations from *Arabidopsis* were obtained from 40 g of leaves, and stromal and lumenal protein extracts were isolated as previously described (Kieselbach *et al*., 1998).

The analyses of the protein fractions were performed in duplicate, in which one replica was stained with Coomassie Blue, and the other was used for the immunoblot analyses. For the latter analyses, 100 µg of stromal protein or 30 µg of lumenal protein

extracts were electrophoresed on 12 % acrylamide gels before transfer to polyvinylidene fluoride membranes (Immun-Blot PVDF, Bio-Rad) according to manufacturer's instructions. The custom-made polyclonal anti-recombinant CS26 antibody (Biomedal S.L., Sevilla, Spain) and secondary antibodies were diluted 1:30.000 and 1:10.000, respectively, in phosphate-buffered saline containing 0.1 % Tween 20 (Sigma-Aldrich) and 5% (w/v) milk powder. Anti-Rubisco activase and anti-PsbO antibodies were used as markers of cross-contamination between the stromal and lumenal extracts, respectively. The ECL Advance Immunoblotting Detection System (GE Healthcare) was used to detect the proteins with horseradish peroxidase-conjugated anti-rabbit secondary antibodies.

Two-Dimensional Electrophoresis

The lumenal proteins (100 μg) were separated by isoelectric focusing in the first dimension and by SDS-PAGE in the second dimension according to Schubert *et al*. (2002) (Schubert *et al*., 2002), with the following modifications: the lumenal proteins were solubilised in 8 M urea, 2 % (w/v) CHAPS (3-[3-cholamidopropyl) dimethylammonio]-1-propanesulfonic acid), 50 mM dithiothreitol, 0.2 % (v/v) ampholytes (Bio-Lyte 3-10 buffer, Bio-Rad) and a trace of bromophenol blue, and applied during rehydration to a linear IPG strip, pH 4-7.

Isoelectrofocusing was performed at 22 °C in the Protean IEF Cell (Bio-Rad) in three steps: S1: 250 V for 15 min, S2: 10000 V for 1 h and S3: 10000 V up to 40000 V. Intensity was fixed to 50 μA/strip IPG2 to avoid the overheating of the system.

Prior to the second dimension, the gel strips were equilibrated for 2 × 15 min in a solution containing 6 M urea, 20 % (v/v) glycerol, 2 % (w/v) SDS, and 0.4 M Tris-HCl, pH 8.8, with 50 mM DTT added to the first equilibration solution and 2.5 % (w/v) iodoacetamide to the second. The gel strips were washed with a solution containing 25 mM Tris-HCl, pH 8.3, 0.2 M glycine and 0.1 % SDS (w/v).

The equilibrated gel strips were placed on top of vertical polyacrylamide gels (12 % acrylamide and SDS) (Laemmli, 1970). A denaturing solution (0.5 % [w/v] low-melting-point agarose, 0.1 % [w/v] SDS, 0.25 M Tris-HCl, 0.2 M glycine and a trace of bromophenol blue) was loaded on gel strips. Electrophoresis was carried out at 240 V and 35 mA/gel for 5 h using the Protean II xi Cell (Bio-Rad).

The gels were stained with silver nitrate using the Silver Staining Kit, Protein (GE Healthcare) according to manufacturer's instruction. The two-dimensional silver-stained

gels were scanned with a GS-800 Densitometer (Bio-Rad). Image analyses were conducted with the PDQuest 8.0 2-D Analysis Software (Bio-Rad).

Protein Identification by Mass Spectrometry

Spots of interest were excised from the stained one- or two-dimensional gels using an ExQuest Spot Cutter System (Bio-Rad). The stain was eliminated by the incubation of the bands with acetonitrile for 10 min and vacuum drying for 15 min. The spots were digested by 0.013 μg/μL trypsin and 50 mM NH_4HCO_3, pH 7.8. After incubation for 30 min at 4 ºC, the supernatant was removed, and 10 μM of 50 mM NH_4HCO_3, pH 7.8, was added and incubated for 15 h at 37 ºC. The reaction was stopped by the addition of 0.5 % (v/v) trichloroacetic acid. After digestion, the peptide mass fingerprint data was collected by a MALDI-mass spectrometry analysis on an Autoflex MALDI-TOF mass spectrometer (Bruker Daltonics, Bremen, Germany). Before each analysis, the instrument was externally calibrated using the Peptide Calibration Standard (Bruker Daltonics). Proteins were identified according to the highest-ranked result by searching the NCBI non-redundant protein sequence database using the MASCOT search engine (Matrix Science, Boston, USA). Searching parameters included the carbamidomethylation of cysteines and methionine oxidation.

Statistical Analysis

A univariate analysis of variance (ANOVA) was performed to reveal the differences between genotypes and photoperiods for the studied parameters. The analyses were performed using the Origin Pro 7.5 software package (Originlab Corporation, Massachusett, USA). Comparisons were tested using the Duncan analysis at a significance level of $P < 0.05$. When possible, a significance level of $P < 0.01$ was applied. If required, multiple comparison tests were used by the application of Duncan's multiple range test at a significance level of $P < 0.05$ (or $P < 0.01$) for the analysis of mean differences using Statgraphics Centurion (Statpoint Technologies, Inc., Virginia, USA).

ACKNOWLEDGMENTS

M.A.B. is grateful to Junta de Andalucía for her fellowship support and to EMBO for a short-term fellowship. We thank Dr. Marika Lindahl and Dr. María Cruz González for providing us with the anti-PsbO and anti-Rubisco activase antibodies and Rocío Rodríguez from the IBVF Protein Analysis Service for the protein identification by mass spectrometry.

LITERATURE CITED

Aldridge C, Cain P, Robinson C (2009) Protein transport in organelles: Protein transport into and across the thylakoid membrane. FEBS J **276:** 1177-1186

Asada K (1999) THE WATER-WATER CYCLE IN CHLOROPLASTS: Scavenging of Active Oxygens and Dissipation of Excess Photons. Annu Rev Plant Physiol Plant Mol Biol **50:** 601-639

Baker NR (2008) Chlorophyll fluorescence: a probe of photosynthesis in vivo. Annu Rev Plant Biol **59:** 89-113

Bermudez MA, Paez-Ochoa MA, Gotor C, Romero LC (2010) Arabidopsis S-sulfocysteine synthase activity is essential for chloroplast function and long-day light-dependent redox control. Plant Cell **22:** 403-416

Bernacchi C, Portis A, Nakano H, von Caemmerer S, Long S (2002) Temperature response of mesophyll conductance. Implications for the determination of Rubisco enzyme kinetics and for limitations to photosynthesis in vivo. Plant Physiol **130:** 1992-2000

Bernacchi C, Singsaas E, Pimentel C, Portis Jr A, Long S (2001) Improved temperature response functions for models of Rubisco limited photosynthesis. Plant Cell Environ **24:** 253-512

Bondarava N, Gross CM, Mubarakshina M, Golecki JR, Johnson GN, Krieger-Liszkay A (2010) Putative function of cytochrome b559 as a plastoquinol oxidase. Physiol Plant **138:** 463-473

Boyes DC, Zayed AM, Ascenzi R, McCaskill AJ, Hoffman NE, Davis KR, Gorlach J (2001) Growth stage-based phenotypic analysis of Arabidopsis: a model for high throughput functional genomics in plants. Plant Cell **13:** 1499-1510

Bradford MM (1976) A rapid and sensitive method for the quantitation of microgram quantities of protein utilizing the principle of protein-dye binding. Anal Biochem **72:** 248-254

Buchanan BB, Luan S (2005) Redox regulation in the chloroplast thylakoid lumen: a new frontier in photosynthesis research. J Exp Bot **56:** 1439-1447

Douce R, Neuburger M (1999) Biochemical dissection of photorespiration. Curr Opin Plant Biol **2:** 214-222

Droux M, Ruffet ML, Douce R, Job D (1998) Interactions between serine acetyltransferase and O-acetylserine (thiol) lyase in higher plants--structural and kinetic properties of the free and bound enzymes. Eur J Biochem **255:** 235-245

Ekelund N (2000) Interactions between photosynthesis and 'light-enhanced dark respiration' (LEDR) in the flagellate Euglena gracilis after irradiation with ultraviolet radiation. Journal of photochemistry and photobiology. B, Biology **55:** 63-72

Ethier GH, Livingstone NJ (2004) On the need to incorporate sensitivity to CO2 transfer conductance into the Farquhar-von Caemmerer-Berry leaf photosynthesis model. Plant Cell Environ **27:** 137-153

Farquhar C, Von Caemmerer S (1982) Modelling of photosynthetic response to enviromental condictions. Physiological Plant Ecology II. (O.L. Lange, P.S. Nobel, C.B. Osmond and H. Ziegler Eds). Springer-Verlag Berlin**:** 549-587

Farquhar GD, Von Caemmerer S, Berry JA (1980) A biochemicall model of photsynthetic CO2 assimilation in leaves of C3 species. Planta **149:** 78-90

Flexas J, Diaz-Espejo A, Berry JA, Cifre J, Galmes J, Kaldenhoff R, Medrano H, Ribas-Carbo M (2007) Analysis of leakage in IRGA's leaf chambers of open gas exchange systems: quantification and its effects in photosynthesis parameterization. J Exp Bot **58:** 1533-1543

Flexas J, Diaz-Espejo A, Galmes J, Kaldenhoff R, Medrano H, Ribas-Carbo M (2007) Rapid variations of mesophyll conductance in response to changes in CO2 concentration around leaves. Plant Cell Environ **30:** 1284-1298

Flexas J, Ortuno MF, Ribas-Carbo M, Diaz-Espejo A, Florez-Sarasa ID, Medrano H (2007) Mesophyll conductance to CO2 in Arabidopsis thaliana. New Phytol **175:** 501-511

Fristedt R, Vener AV (2011) High Light Induced Disassembly of Photosystem II Supercomplexes in Arabidopsis Requires STN7-Dependent Phosphorylation of CP29. PLoS ONE **6:** e24565

Galmés J, Conesa M, Ochogavía J, Perdomo J, Francis D, Ribas-Carbó M, Savé R, Flexas J, Medrano H, Cifre J (2011) Physiological and morphological adaptations in relation to water use efficiency in Mediterranean accessions of Solanum lycopersicum. Plant Cell Environ **34:** 245-305

Galmes J, Medrano H, Flexas J (2006) Acclimation of Rubisco specificity factor to drought in tobacco: discrepancies between in vitro and in vivo estimations. J Exp Bot **57:** 3659-3667

Genty B, Briantais JM, Baker NR (1989) The relationship between the quantum yield of photosynthetic electron transport and quenching of chlorophyll fluorescence. Biochimica et Biophysica Acta (BBA)-General Subjects **990:** 87-179

Gilbert GH, Antonson DE, Mjor IA, Ringelberg ML, Dolan TA, Foerster U, Legler DW, Heft MW, Duncan RP (1996) Coronal caries, root fragments, and restoration and cusp fractures in US adults. Caries Res **30:** 101-111

Gopalan G, He Z, Balmer Y, Romano P, Gupta R, Heroux A, Buchanan BB, Swaminathan K, Luan S (2004) Structural analysis uncovers a role for redox in regulating FKBP13, an immunophilin of the chloroplast thylakoid lumen. Proc Natl Acad Sci U S A **101:** 13945-13950

Gutensohn K, Magens M, Kruger W, Kroger N, Kuhnl P (2006) Comparison of flow cytometry vs. a haematology cell analyser-based method to guide the optimal time-point for peripheral blood stem cell apheresis. Vox Sang **90:** 53-58

Harley PC, Loreto F, Di Marco G, Sharkey TD (1992) Theoretical Considerations when Estimating the Mesophyll Conductance to CO(2) Flux by Analysis of the Response of Photosynthesis to CO(2). Plant Physiol **98:** 1429-1436

Horton P, Ruban AV, Walters RG (1996) Regulation of Light Harvesting in Green Plants. Annu Rev Plant Physiol Plant Mol Biol **47:** 655-684

Howarth JR, Dominguez-Solis JR, Gutierrez-Alcala G, Wray JL, Romero LC, Gotor C (2003) The serine acetyltransferase gene family in Arabidopsis thaliana and the regulation of its expression by cadmium. Plant Mol Biol **51:** 589-598

Kapri-Pardes E, Naveh L, Adam Z (2007) The Thylakoid Lumen Protease Deg1 Is Involved in the Repair of Photosystem II from Photoinhibition in Arabidopsis. The Plant Cell Online **19:** 1039-1047

Karamoko M, Cline S, Redding K, Ruiz N, Hamel PP (2011) Lumen Thiol Oxidoreductase1, a Disulfide Bond-Forming Catalyst, Is Required for the Assembly of Photosystem II in Arabidopsis. The Plant Cell Online **23:** 4462-4475

Kidner C, Sundaresan V, Roberts K, Dolan L (2000) Clonal analysis of the Arabidopsis root confirms that position, not lineage, determines cell fate. Planta **211:** 191-199

Kieselbach T, Hagman, Andersson B, Schroder WP (1998) The thylakoid lumen of chloroplasts. Isolation and characterization. J Biol Chem **273:** 6710-6716

Kim CM, Park SH, Je BI, Park SJ, Piao HL, Eun MY, Dolan L, Han CD (2007) OsCSLD1, a cellulose synthase-like D1 gene, is required for root hair morphogenesis in rice. Plant Physiol **143:** 1220-1230

Kim Y, Steudle E (2007) Light and turgor affect the water permeability (aquaporins) of parenchyma cells in the midrib of leaves of Zea mays. J Exp Bot **58:** 4119-4148

Komenda J, Nickelsen J, Tichý M, Prášil O, Eichacker LA, Nixon PJ (2008) The Cyanobacterial Homologue of HCF136/YCF48 Is a Component of an Early Photosystem II Assembly Complex and Is Important for Both the Efficient Assembly and Repair of Photosystem II in Synechocystis sp. PCC 6803. J Biol Chem **283:** 22390-22399

Koussevitzky S, Nott A, Mockler TC, Hong F, Sachetto-Martins G, Surpin M, Lim J, Mittler R, Chory J (2007) Signals from chloroplasts converge to regulate nuclear gene expression. Science **316:** 715-719

Laemmli UK (1970) Cleavage of structural proteins during the assembly of the head of bacteriophage T4. Nature **227:** 680-685

Lepistö A, Kangasjärvi S, Luomala E-M, Brader G, Sipari N, Keränen M, Keinänen M, Rintamäki E (2009) Chloroplast NADPH-thioredoxin reductase interacts with photoperiodic development in Arabidopsis. Plant Physiol **149:** 1261-1337

Loreto F, Tsonev T, Centritto M (2009) The impact of blue light on leaf mesophyll conductance. J Exp Bot **60:** 2283-2373

Lundquist P, Poliakov A, Bhuiyan NH, Zybailov B, Sun Q, van Wijk KJ (2012) The functional network of the Arabidopsis thaliana plastoglobule proteome based on quantitative proteomics and genome-wide co-expression analysis. Plant Physiol

Mahler H, Wuennenberg P, Linder M, Przybyla D, Zoerb C, Landgraf F, Forreiter C (2007) Singlet oxygen affects the activity of the thylakoid ATP synthase and has a strong impact on its gamma subunit. Planta **225:** 1073-1083

Meurer J, Plucken H, Kowallik KV, Westhoff P (1998) A nuclear-encoded protein of prokaryotic origin is essential for the stability of photosystem II in Arabidopsis thaliana. EMBO J **17:** 5286-5297

Moskvin O, Ivanov B, Ignatova L, Kollmeier M (2000) Light-induced stimulation of carbonic anhydrase activity in pea thylakoids. FEBS Lett **470:** 375-382

Muhlenbock P, Szechynska-Hebda M, Plaszczyca M, Baudo M, Mateo A, Mullineaux PM, Parker JE, Karpinska B, Karpinski S (2008) Chloroplast signaling and LESION SIMULATING DISEASE1 regulate crosstalk between light acclimation and immunity in Arabidopsis. Plant Cell **20:** 2339-2356

Muller P, Li XP, Niyogi KK (2001) Non-photochemical quenching. A response to excess light energy. Plant Physiol **125:** 1558-1566

Munn, Bosch S, Alegre L (2004) Die and let live: leaf senescence contributes to plant survival under drought stress. Functional Plant Biology **31:** 203-216

Murakami R, Ifuku K, Takabayashi A, Shikanai T, Endo T, Sato F (2002) Characterization of an Arabidopsis thaliana mutant with impaired psbO, one of two genes encoding extrinsic 33-kDa proteins in photosystem II. FEBS Lett **523:** 138-142

Neta P, Huie RE (1985) Free-radical chemistry of sulfite. Environ Health Perspect **64:** 209-217

Nixon PJ, Michoux F, Yu J, Boehm M, Komenda J (2010) Recent advances in understanding the assembly and repair of photosystem II. Ann Bot (Lond) **106:** 1-16

Padmasree K, Padmavathi L, Raghavendra A (2002) Essentiality of mitochondrial oxidative metabolism for photosynthesis: optimization of carbon assimilation and protection against photoinhibition. Critical reviews in biochemistry and molecular biology **37:** 71-190

Peltier JB, Emanuelsson O, Kalume DE, Ytterberg J, Friso G, Rudella A, Liberles DA, Soderberg L, Roepstorff P, von Heijne G, van Wijk KJ (2002) Central functions of the lumenal and peripheral thylakoid proteome of Arabidopsis determined by experimentation and genome-wide prediction. Plant Cell **14:** 211-236

Pesaresi P, Hertle A, Pribil M, Kleine T, Wagner R, Strissel H, Ihnatowicz A, Bonardi V, Scharfenberg M, Schneider A, Pfannschmidt T, Leister D (2009) Arabidopsis STN7 kinase provides a link between short- and long-term photosynthetic acclimation. Plant Cell **21:** 2402-2423

Plücken H, Müller B, Grohmann D, Westhoff P, Eichacker LA (2002) The HCF136 protein is essential for assembly of the photosystem II reaction center in Arabidopsis thaliana. FEBS Lett **532:** 85-90

Pogson BJ, Woo NS, Forster B, Small ID (2008) Plastid signalling to the nucleus and beyond. Trends Plant Sci **13:** 602-609

Raghavendra A, Padmasree K (2003) Beneficial interactions of mitochondrial metabolism with photosynthetic carbon assimilation. Trends Plant Sci **8:** 546-599

Reddy M, Vani T, Raghavendra A (1991) Light-enhanced dark respiration in mesophyll protoplasts from leaves of pea. Plant Physiol **96:** 1368-1439

Robinson C, Thompson SJ, Woolhead C (2001) Multiple pathways used for the targeting of thylakoid proteins in chloroplasts. Traffic **2:** 245-251

Sam O, Ramírez C, Coronado MJ, Testillano PS, Risueño MC (2003) Changes in Tomato Leaves Induced by NaCl Stress: Leaf Organization and Cell Ultrastructure. Biologia Plantarum **47:** 361-366

Saradadevi K, Raghavendra A (1992) Dark Respiration Protects Photosynthesis Against Photoinhibition in Mesophyll Protoplasts of Pea (Pisum sativum). Plant Physiol **99:** 1232-1239

Schubert M, Petersson U, Haas B, Funk C, Schröder W, Kieselbach T (2002) Proteome map of the chloroplast lumen of Arabidopsis thaliana. J Biol Chem **277:** 8354-8419

Sharkey TD, Bernacchi CJ, Farquhar GD, Singsaas EL (2007) Fitting photosynthetic carbon dioxide response curves for C(3) leaves. Plant Cell Environ **30:** 1035-1040

Singh KK, Shyam R, Sane PV (1996) Reactivation of photosynthesis in the photoinhibited green alga Chlamydomonas reinhardtii: role of dark respiration and of light. Photosynth Res **49:** 11-31

Stessman D, Miller A, Spalding M, Rodermel S (2002) Regulation of photosynthesis during Arabidopsis leaf development in continuous light. Photosynth Res **72:** 27-37

Vidi P-A, Kanwischer M, Baginsky S, Austin JR, Csucs G, Dörmann P, Kessler F, Bréhélin C (2006) Tocopherol Cyclase (VTE1) Localization and Vitamin E Accumulation in Chloroplast Plastoglobule Lipoprotein Particles. J Biol Chem **281:** 11225-11234

Warren CR, Dreyer E (2006) Temperature response of photosynthesis and internal conductance to CO2: results from two independent approaches. J Exp Bot **57:** 3057-3067

Watanabe M, Kusano M, Oikawa A, Fukushima A, Noji M, Saito K (2008) Physiological roles of the beta-substituted alanine synthase gene family in Arabidopsis. Plant Physiol **146:** 310-320

Wirtz M, Droux M, Hell R (2004) O-acetylserine (thiol) lyase: an enigmatic enzyme of plant cysteine biosynthesis revisited in Arabidopsis thaliana. J Exp Bot **55:** 1785-1798

Wirtz M, Hell R (2006) Functional analysis of the cysteine synthase protein complex from plants: structural, biochemical and regulatory properties. J Plant Physiol **163:** 273-286

Zell M, Fahnenstich H, Maier A, Saigo M, Voznesenskaya E, Edwards G, Andreo C, Schleifenbaum F, Zell C, Drincovich M, Maurino V (2010) Analysis of Arabidopsis with highly reduced levels of malate and fumarate sheds light on the role of these organic acids as storage carbon molecules. Plant Physiol **152:** 1251-1313

Zhang N, Kallis R, Ewy R, Portis A (2002) Light modulation of Rubisco in Arabidopsis requires a capacity for redox regulation of the larger Rubisco activase isoform. Proc Natl Acad Sci U S A **99:** 3330-3334

Zybailov B, Rutschow H, Friso G, Rudella A, Emanuelsson O, Sun Q, van Wijk KJ (2008) Sorting signals, N-terminal modifications and abundance of the chloroplast proteome. PLoS One **3:** e1994

FIGURE LEGENDS

Figure 1. Phenotypic characterisation of wild-type and mutant *cs26* under the two photoperiods. A, Leaves from plants that were grown for 3 weeks under long-day conditions. B, Leaves from plants that were grown for 5 weeks under short-day conditions. C, Leaf mass area (LMA). Values are means ± SD (n = 5). * Significant differences at $P < 0.05$ between wild-type and *cs26* under a given photoperiod. † Significant differences at $P < 0.05$ between plants of the same genotype grown under the two photoperiods.

Figure 2. Photosynthetic rates for the wild-type and *cs26* plants. Determination of the net CO_2 assimilation rate (A_N) at varying substomatal (C_i) or chloroplast (C_c) CO_2 concentration were performed for wild-type (black squares) and *cs26* (white diamonds) plants of *Arabidopsis thaliana* under short-day (A, C) and long-day (B, D) growth conditions. The values are averages ±SE of 6 replicates per genotype, photoperiod and CO_2 concentration.

Figure 3. Light-response curves in wild-type (black squares) and *cs26* (white diamonds) under long-day photoperiod. A, The response of net CO_2 assimilation rate (A_N) to

photosynthetic active radiation (PAR), B, the response of electron transport rate (J) to absorbed PAR (PAR_{abs}), and C, the relationship between J and gross CO_2 assimilation rate (A_G), A_G being the sum of A_N and light respiration (R_L). PAR_{abs} was obtained by correcting the incoming PAR intensities with the leaf absorbance, which was taken from the product of $\alpha \cdot \beta$, considering β as constant and equal to 0.5. In Figure 3C, the regression lines for wild-type (solid lines) and *cs26* (dashed lines) are shown. The values are averages ± SD for 6 replicates per genotype and photoperiod.

Figure 4. Representative whole-rosette chlorophyll fluorescence images. Images for the maximum quantum efficiency of photosystem II (F_v/F_m) that were obtained from the wild-type (wt) and *cs26* plants that were grown for 5 weeks under the short-day photoperiod, A, and for 3 weeks under the long-day photoperiod, B. Images for non-photochemical quenching (NPQ) under short-day and long-day at a PPFD of 150 for C and D, respectively, and 800 μmol m^{-2} s^{-1} for E and F, respectively. Colour scales for each parameter are shown.

Figure 5. Expression levels of *CS26* in wild-type plants. Real-time RT-PCR analysis of the expression of the *CS26* gene was performed at different stages in the development of soil-grown wild type plants. The transcript levels were normalised using the constitutive *UBQ10* gene as an internal control. At each developmental stage, leaves from the rosettes were analysed with the exception of stage 6.1, at which the stems and flowers were also analysed (S+F). Data shown are means ± SD of three independent analyses using RNA that was obtained from different plants that were grown in separate pots at the same time.

Figure 6. Localisation of CS26 and OAS-B proteins in chloroplast of *Arabidopsis*
Stroma and lumen preparations from *Arabidopsis* were isolated from 40 g of leaves of wild type and *oas-b* and *cs26* mutant plants that were grown for 5 weeks under short-day conditions. In all, 100 μg of stromal or 30 μg of lumenal protein extracts was electrophoresed on 12 % acrylamide gels. One replica was stained with Coomassie Blue, A and C, and the second was used for immunoblot analyses using anti-CS26 antibodies, B and D. Proteins identified by MALDI-TOF were: RBCL (Rubisco large subunit), RCA (Rubisco activase), GAP-A (glyceraldehyde 3-phosphate dehydrogenase A subunit), PGK1 (phosphoglycerate kinase 1), FBA (fructose-bisphosphatealdolase, class I), FNR (ferredoxin-NADP(H) oxidoreductase), PsbO (oxygen-evolving enhancer), TL29 (ascorbate

peroxidase 4), DegP1 (DEG protease 1), HCF136 (high chlorophyll fluorescence 136), TLP38 (cyclophilin 38). Specific bands for the OAS-B and CS26 proteins that were detected by the antibody are shown. MW: molecular weight markers.

Figure 7. S-sulfocysteine synthase activity in stromal and lumenal fractions under long-day, A, and short-day, B, conditions**.** SSCS activity was measured in stromal (white columns) and lumenal (black columns) fraction extracts from the chloroplasts of the wild-type and the *oas-b* and *cs26* mutant lines. Values are means ±SD of three independent determinations. Significant differences between mutants and wild type in the stromal fraction are indicated by the letter *a* ($P< 0.05$). Significant differences between mutants and wild type in the lumenal fractions are indicated by the letter *b* ($P < 0.05$).

Supplemental Data

Supplemental Figure S1. Cross-contamination between stromal and lumenal fraction. Stromal and lumenal preparations from *Arabidopsis* were isolated from 40 g of leaves from wild type and *oas-b* and *cs26* mutant plants. To avoid signal saturation of Rubisco activase protein in the stromal extract, only 0.6 μg of stromal protein extracts, A-B, were loaded, and from the lumenal extract, 30 μg of protein, C-D, were loaded. All samples were electrophoresed on 12 % acrylamide gels and used for immunoblot analyses using anti-Rbc activase and anti-PsbO antibodies. A, In the stromal fraction, two bands at 47 and 42 kDa, corresponding with Rubisco activase were observed in all lines with the α-Rbc activase antibody. B, Weak band at 33 kDa corresponding with PsbO was also detected in the stromal extract when α-PsbO was used. There was no signal detection when α-Rbc activase was used in the lumenal extracts.

Supplemental Figure S2. Proteome map of the chloroplast lumen of the wild type and mutant *cs26*. Silver-stained two-dimensional gels of 100 μg soluble lumenal proteins from the chloroplasts of 4-week-old plants that were grown in long-day conditions are shown. The proteins were resolved by SDS electrophoresis in a 12% polyacrylamide gel subsequent to isoelectrofocusing in a linear immobilised pH gradient from pH 4 to 7. The circles denote protein spot differences that were identified by MALDI-TOF. See Table V for detailed information on each identified protein.

Table I. *Photosynthetic characterisation of wild-type and* cs26 *plants grown under long-day or short-day photoperiod*

Net CO_2 assimilation rate (A_N), stomatal conductance (g_s), photosynthetic water-use efficiency (A_N/g_s), mesophyll conductance (g_m), ratio of mesophyll and stomatal conductances to CO_2 (g_m/g_s), CO_2 concentration at the site of carboxylation (C_c), CO_2 compensation point on a C_c-basis (Γ_{Cc}), maximum velocity of carboxylation ($V_{c,max}$), maximum capacity of electron transport (J_{max}), ratio between maximum rates of electron transport and carboxylation ($J_{max}/V_{c,max}$), and mitochondrial respiration (R_{dark}) and g_s at darkness ($g_{s,dark}$) are shown. Values represent means ± SD (n = 6). A_N, g_s, A_N/g_s, g_m, g_m/g_s and C_c were obtained from steady-state measurements at a PAR of 1000 μmol m^{-2} s^{-1} and C_a of 400 μmol mol^{-1}. The g_m and C_c values were estimated according to the variable *J* method and used to convert the A_N-C_i curves into A_N-C_c. Γ_{Cc_based}, $V_{c,max}$ and J_{max} were taken from the A_N-C_c curves. R_{dark} and $g_{s,dark}$ were obtained from measurements at darkness and a C_a of 400 μmol mol^{-1}. The significant differences between the *cs26* mutant and wild-type grown under the same photoperiod are indicated by the letter *a* ($P < 0.05$). Significant differences between the long-day and short-day photoperiod-grown plants for the same genotype are indicated by the letter *b* ($P < 0.05$).

	Long-day		Short-day	
	wild-type	*cs26*	wild-type	*cs26*
A_N (μmol CO_2 m^{-2} s^{-1})	8.3 ± 0.3	1.9 ± 0.3 [a]	11.6 ± 0.9[b]	11.1 ± 0.5[b]
g_s (mol H_2O m^{-2} s^{-1})	0.20 ± 0.07	0.18 ± 0.08	0.17 ± 0.01	0.18 ± 0.02
A_N/g_s (μmol CO_2 mol^{-1} H_2O)	41.4 ± 0.8	10.4 ± 0.5 [a]	68.1 ± 4.1 [b]	61.8 ± 6.2[b]
g_m (mol CO_2 m^{-2} s^{-1})	0.42 ± 0.09	0.01 ± 0.01 [a]	0.10 ± 0.03 [b]	0.14 ± 0.05[b]
g_m/g_s (mol CO_2 mol^{-1} H_2O)	2.05± 0.06	0.05± 0.01 [a]	0.58± 0.12 [b]	0.78± 0.14[b]
C_c (μmol CO_2 mol^{-1} air)	374 ± 34	340 ± 20	230 ± 23 [b]	295 ± 10 [a,b]
R_{dark} (μmol CO_2 m^{-2} s^{-1})	-1.01 ± 0.25	-1.77 ± 0.33 [a]	-0.56 ± 0.29 [b]	-0.57 ± 0.10 [b]
$g_{s.dark}$ (mol H_2O m^{-2} s^{-1})	0.27 ± 0.13	0.28 ± 0.06	0.05 ± 0.01 [b]	0.07 ±0.02 [b]
$V_{c,max}$ (μmol CO_2m^{-2} s^{-1})	24.6 ± 2.6	9.0 ± 2.3 [a]	41.0 ± 5.0 [b]	31.6 ± 1.4[a,b]
J_{max} (μmol CO_2m^{-2} s^{-1})	48.6 ± 2.5	17.3 ± 5.1 [a]	80.7 ± 12.1 [b]	74.9 ± 4.7[b]
$J_{max}/V_{c,max}$	2.0 ± 0.2	1.9 ± 0.4	2.0 ± 0.1	2.4 ± 0.1[a,b]
Γ_{Cc} (μmol CO_2 mol^{-1} air)	51.0 ± 2.6	119.0 ± 10.0 [a]	42.8 ± 1.6 [b]	42.0 ± 1.6[b]

Table II. *Total soluble protein and Rubisco concentrations*

Leaf extracts from wild-type and *cs26* plants grown under the two photoperiods were obtained. The total soluble protein [TSP] was determined by the method of Bradford and the Rubisco concentrations by SDS-PAGE titration as described in Materials and Methods. Values are averages ± SE (n = 3). Significant differences between wild-type and *cs26* within the same photoperiod are indicated by the letter *a* ($P < 0.05$). Significant differences between long- and short-day-grown plants within the same genotype are indicated by the letter *b* ($P < 0.05$). LD: long-day photoperiod; SD: short-day photoperiod.

	[TSP] (µg/µL)		[Rubisco] (µg/µL)		[Rubisco]/[TSP]	
	LD	SD	LD	SD	LD	SD
wild-type	4.00 ± 0.28	4.17 ± 0.02	1.06 ± 0.05	0.85 ± 0.02 [b]	0.27 ± 0.02	0.20 ± 0.01 [b]
cs26	3.10 ± 0.07 [a]	3.87 ± 0.12 [b]	0.31 ± 0.01 [a]	0.72 ± 0.13 [b]	0.10 ± 0.01 [a]	0.18 ± 0.03 [b]

Table III. *Photosynthetic parameters derived from light-response curves in wild-type and cs26 plants under long-day photoperiod*

J, electron transport rate; A_G, gross CO_2 assimilation rate (sum of net CO_2 assimilation rate (A_N) and light respiration (R_L)); PAR_{abs}, absorbed photosynthetic active radiation; and NPQ, non-photochemical quenching are shown. *J*, J/A_G, NPQ and PAR_{abs}/J values were obtained at saturating light intensities (2000 μE m^{-2} s^{-1}). PAR_{abs} was obtained by correcting the incoming PAR intensities with the leaf absorbance, which was taken from the product of α · β, considering β as constant and equal to 0.5. The values are averages ± SE for 6 replicates per genotype. An asterisk indicates significant differences at $P < 0.05$ between the wild-type and *cs26* mutant lines.

	wild-type	***cs26***
J (μmol e^- m^{-2} s^{-1})	48.1 ± 2.3	12.9 ± 3.9*
Inflection point (μmolm^{-2} s^{-1})	533 ± 25	234 ± 56*
Light compensation point (μmol m^{-2} s^{-1})	15.4 ± 6.6	51.3 ± 7.2*
1/Quantum yield (mol h*v* mol^{-1} CO_2)	16.3 ± 1.1	23.6 ± 1.4*
PAR_{abs}/J (mol h*v* mol^{-1} e^-)	3.5 ± 0.1	7.8 ± 0.9*
J/A_G (mol e^- mol^{-1} CO_2)	5.3 ± 0.1	7.7 ± 0.8*
NPQ	1.2 ± 0.2	2.8 ± 0.7*

Table IV. *Photosynthetic parameters from light-adapted wild-type and cs26 plants calculated by chlorophyll fluorescence imaging system*

Measurements were made at two different PPDF levels (150 and 800 μmol m^{-2} s^{-1}). F_q'/F_m', PSII operating efficiency; F_v'/F_m', PSII maximum efficiency; *qP,* PSII efficiency factor; *qL,* fraction of open PSII centres; and NPQ, non-photochemical quenching are shown. The values are averages ± SE of three values at each actinic light for 3 replicates per line. Significant differences between genotypes that were grown under the same photoperiod are indicated by the letter *a* ($P < 0.01$). Significant differences between long- and short-day-grown plants within the same genotype are indicated by the letter *b* ($P < 0.01$).

	Long-day			
	150 μmol m^{-2} s^{-1}		800 μmol m^{-2} s^{-1}	
Parameter	wild-type	*cs26*	wild-type	*cs26*
F_q'/F_m'	0.439 ± 0.024	0.202 ± 0.002[a]	0.314 ± 0.007	0.135 ± 0.001[a]
F_v'/F_m'	0.675 ± 0.002	0.306 ± 0.005[a]	0.529 ± 0.004	0.331 ± 0.021[a]
qP	0.649 ± 0.036	0.611 ± 0.001	0.592 ± 0.015	0.435 ± 0.038[a]
qL	0.526 ± 0.038	1.252 ± 0.005[a]	0.824 ± 0.035	1.531 ± 0.010[a]
NPQ	0.138 ± 0.008	0.298 ± 0.020[a]	0.620 ± 0.019	0.915 ± 0.051[a]
	Short-day			
	150 μmol m^{-2} s^{-1}		800 μmol m^{-2} s^{-1}	
Parameter	wild-type	*cs26*	wild-type	*cs26*
F_q'/F_m'	0.375 ± 0.013[b]	0.286 ± 0.003[a,b]	0.255 ± 0.006[b]	0.182 ± 0.001[a,b]
F_v'/F_m'	0.639 ± 0.007[b]	0.403 ± 0.002[a,b]	0.454 ± 0.004	0.441 ± 0.002[b]
qP	0.587 ± 0.017[b]	0.734 ± 0.001[a,b]	0.577 ± 0.023	0.515 ± 0.006[a,b]
qL	0.527 ± 0.021	1.001 ± 0.012[a,b]	0.672 ± 0.042[b]	0.760 ± 0.011[a,b]
NPQ	0.172 ± 0.017	0.252 ± 0.029[a]	0.879 ± 0.041[b]	1.012 ± 0.020[a,b]

Table V. *Differential display of lumenal proteins from* cs26 *mutant* vs. *wild-type, analysed by MALDI-TOF*

Identifications, functions and fold changes of the different isolated spots are shown. Fold change is expressed as change in protein expression as calculated by PDQuest 2-D analysis software.

Spot	Protein name	Accession number / Gene locus	Function	Fold Chang
1	ATP synthase CF1 α subunit (thylakoid membrane)	gi 7525018/ATCG00120	Hydrogen ion transporting ATPase activity	0.004
2	ATP synthase CF1 β subunit (thylakoid membrane)	gi 7525040/ ATCG00480	Hydrogen ion transmembrane transporter activity	0
3	C-terminal processing protease	gi 15236628/AT4G17740	Serine-type peptidase activity / D1- processing protease	0
4	Cyclophilin/PPIase TLP38	gi 42564190/AT3G15520	Peptidyl-prolyl cis-trans isomerase activity / immunophilin / protein folding	0.14
5,6	HCF136 (high chlorophyll fluorescence 136)	gi 15237225/AT5G23120	Stability and/or assembly factor of photosystem II	0.03 / 0
7	Deg1 protease	gi 2565436/AT3G27925	Trypsin-like serine protease	0
8	ATLFNR1 (LEAF FNR 1) (stroma /thylakoid membrane)	gi145334919/AT5G66190	Ferredoxin:NADP(H) oxidoreductase / electron transporter	0
9,10, 11	PSBO-1(oxygen-evolving enhancer 33)	gi 15240013/ AT5G66570	Oxygen evolving activity	0.76 / 0-1/ 0.04
12,13	PSBO-2 (photosystem II subunit O-2)	gi 15230324/AT3G50820	Oxygen evolving activity	0 / 0-1
14	Photosystem II reaction centre PsbP family protein	gi 79325123/ AT4G15510	Calcium ion binding	0
15,16	PSBP-1 (oxygen-evolving enhancer protein 2)	gi 15222166/ AT1G06680	Regulation of oxygen evolution	0-1 / 0
17	AAA-type ATPase family protein	gi 18398708/ AT2G18330	ATPase activity	0
18	Immunophilin/FKBP-type PPIase	gi 15224305/ AT2G43560	Peptidyl-prolyl cis-trans isomerase activity / protein folding	0.01

19	Thylakoid lumenal 17.9 kDa protein	gi 15234798/ AT4G24930	Unknown	0.03
20	Thylakoid lumenal 17.4 kDa protein	gi 30696347 /AT5G53490	Unknown	0.01
21	Thylakoid lumenal 15 kDa protein	gi 18406661/ AT2G44920	Unknown	0
22	FIBRILIN 2, FBN2. Plastid-lipid-associated protein PAP (thylakoid membrane)	gi 15227428/ AT2G35490	Structural molecule activity	111.68

FIGURE 1

A **B**

C

	LMA (gm^{-2})	
	wild-type	***cs26***
Long-day	10.2 ±1.2	7.5 ±0.5*
Short-day	9.8 ±1.5	10.8 ±1.1†

Figure 1. Phenotypic characterisation of wild-type and mutant *cs26* under the two photoperiods. A, Leaves from plants that were grown for3 weeks under long-day conditions. B, Leaves from plants that were grown for 5 weeks under short-day conditions. C, Leaf mass area (LMA). Values are means ± SD (n = 5). *Significant differences at $P < 0.05$ between wild-type and *cs26* under a given photoperiod. †Significant differences at $P < 0.05$ between plants of the same genotype grown under different photoperiods.

FIGURE 2

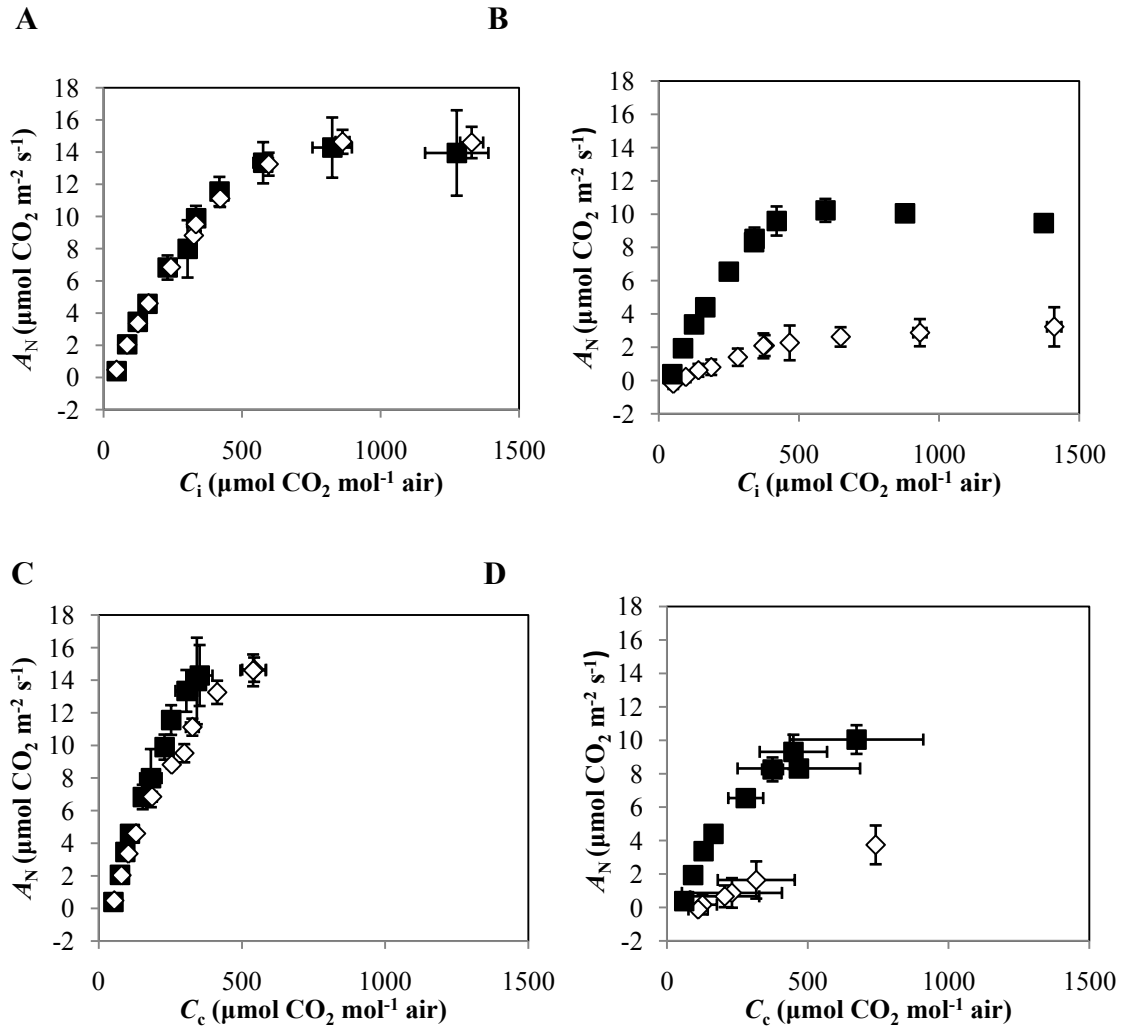

Figure 2. Photosynthetic rates for the wild-type and *cs26* plants. Determination of the net CO_2 assimilation rate (A_N) at varying substomatal (C_i) or chloroplast (C_c) CO_2 concentration were performed for wild-type (black squares) and *cs26* (white diamonds) plants of *Arabidopsis thaliana* under short-day (A, C) and long-day (B, D) growth conditions. The values are averages ±SE of 6 replicates per genotype, photoperiod and CO_2 concentration.

FIGURE 3

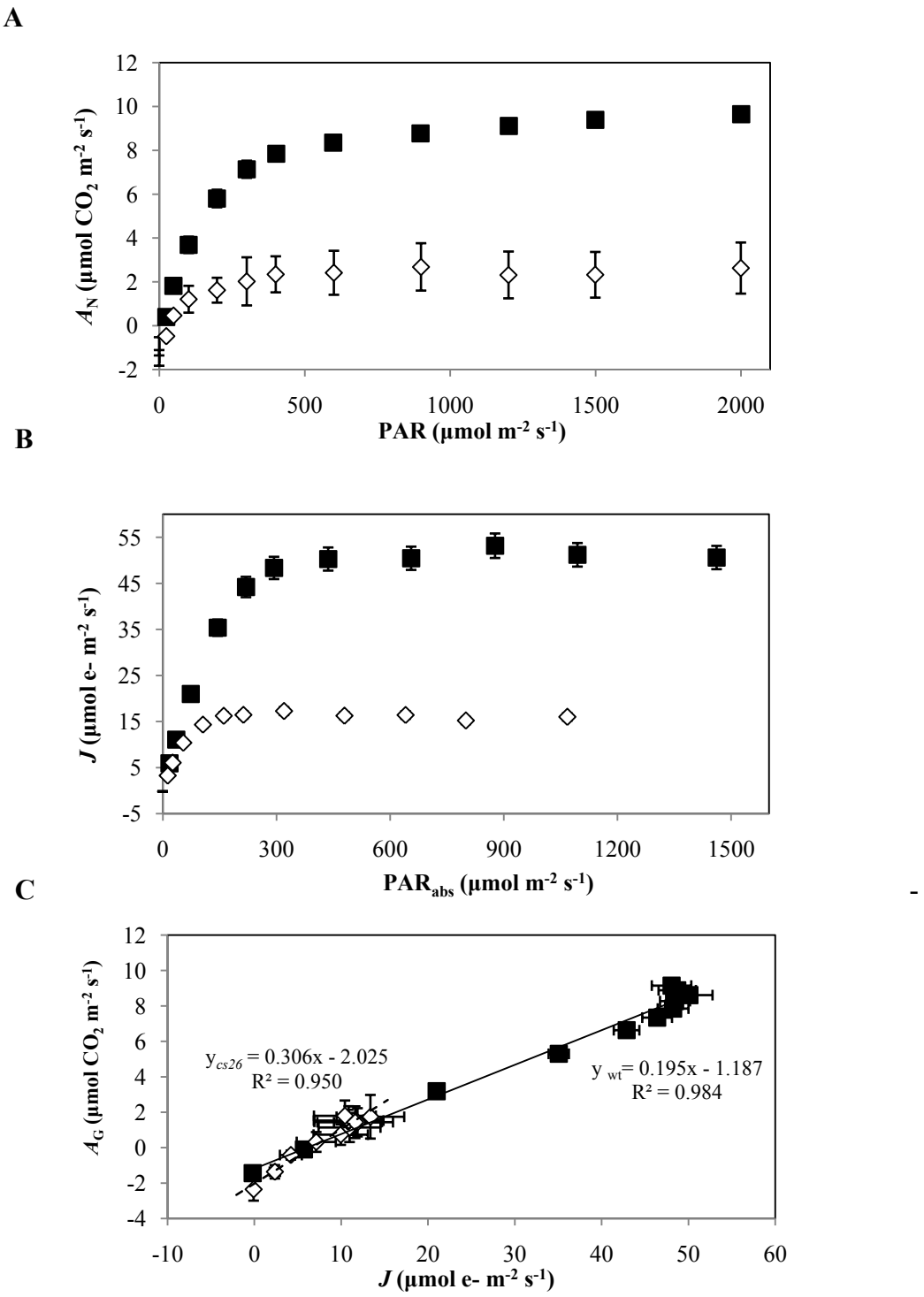

Figure 3. Light-response curves in wild-type (black squares) and *cs26* (white diamonds) under long-day photoperiod. A, The response of net CO_2 assimilation rate(A_N) to photosynthetic active radiation (PAR), B, the response of electron transport rate (J) to absorbed PAR (PAR_{abs}), and C, the relationship between J and gross CO_2 assimilation rate (A_G), A_G being the sum of A_N and light respiration (R_L). PAR_{abs} was obtained by correcting the incoming PAR intensities with the leaf absorbance, which was taken from the product of $\alpha \cdot \beta$, considering β as constant and equal to 0.5. In Figure 3C, the regression lines for wild-type

(solid lines) and *cs26* (dashed lines) are shown. The values are averages ± SD for 6 replicates per genotype and photoperiod.

FIGURE 4

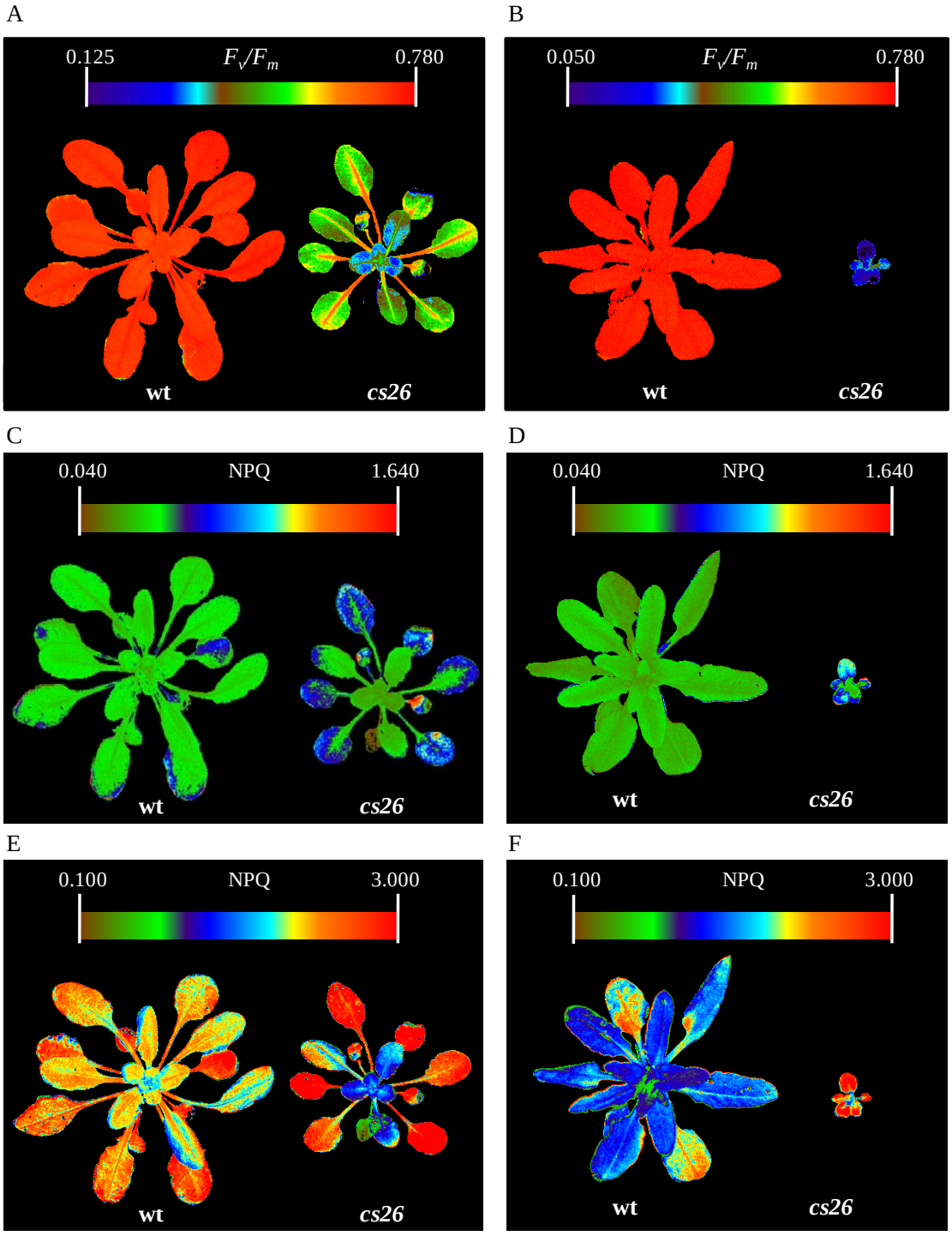

Figure 4. Representative whole-rosette chlorophyll fluorescence images. Images for the maximum quantum efficiency of photosystem II (F_v/F_m) that were obtained from the wild-type (wt) and *cs26* plants that were grown for 5 weeks under the short-day photoperiod, A, and for 3 weeks under the long-day photoperiod, B. Images for non-photochemical quenching (NPQ) under short-day and long-day at a PPFD

of 150 for C and D, respectively, and 800 μmol m^{-2} s^{-1} for E and F, respectively. Colour scales for each parameter are shown.

FIGURE 5

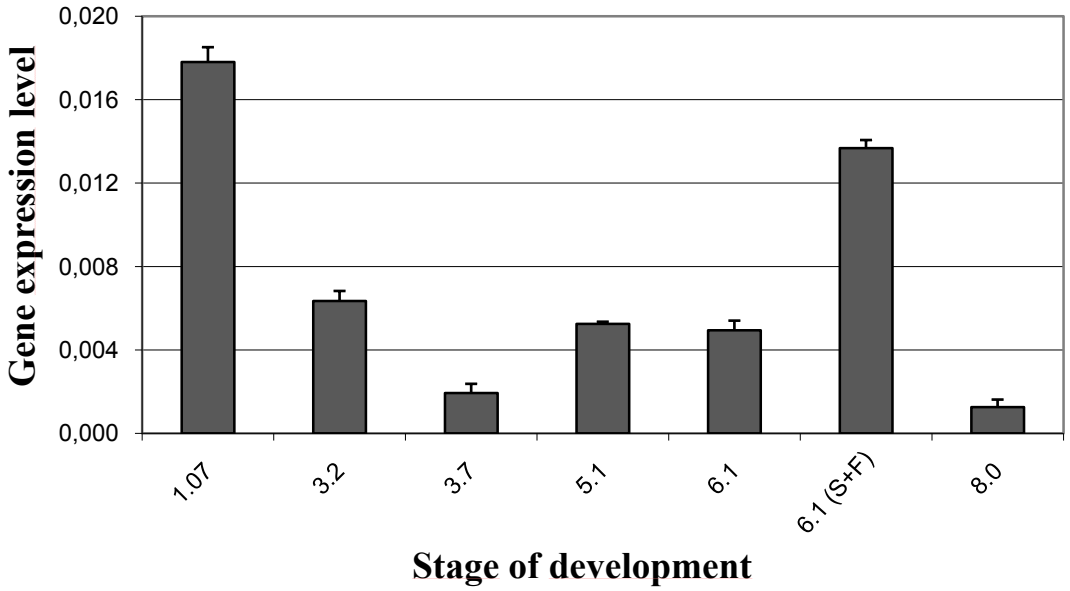

Figure 5. Expression levels of *CS26* in wild-type plants.

Real-time RT-PCR analysis of the expression of the *CS26* gene was performed at different stages in the development of soil-grown wild type plants. The transcript levels were normalised using the constitutive *UBQ10* gene as an internal control. At each developmental stage, leaves from the rosettes were analysed with the exception of stage 6.1, at which the stems and flowers were also analysed (S+F). Data shown are means ± SD of three independent analyses using RNA that was obtained from different plants that were grown in separate pots at the same time.

FIGURE 6

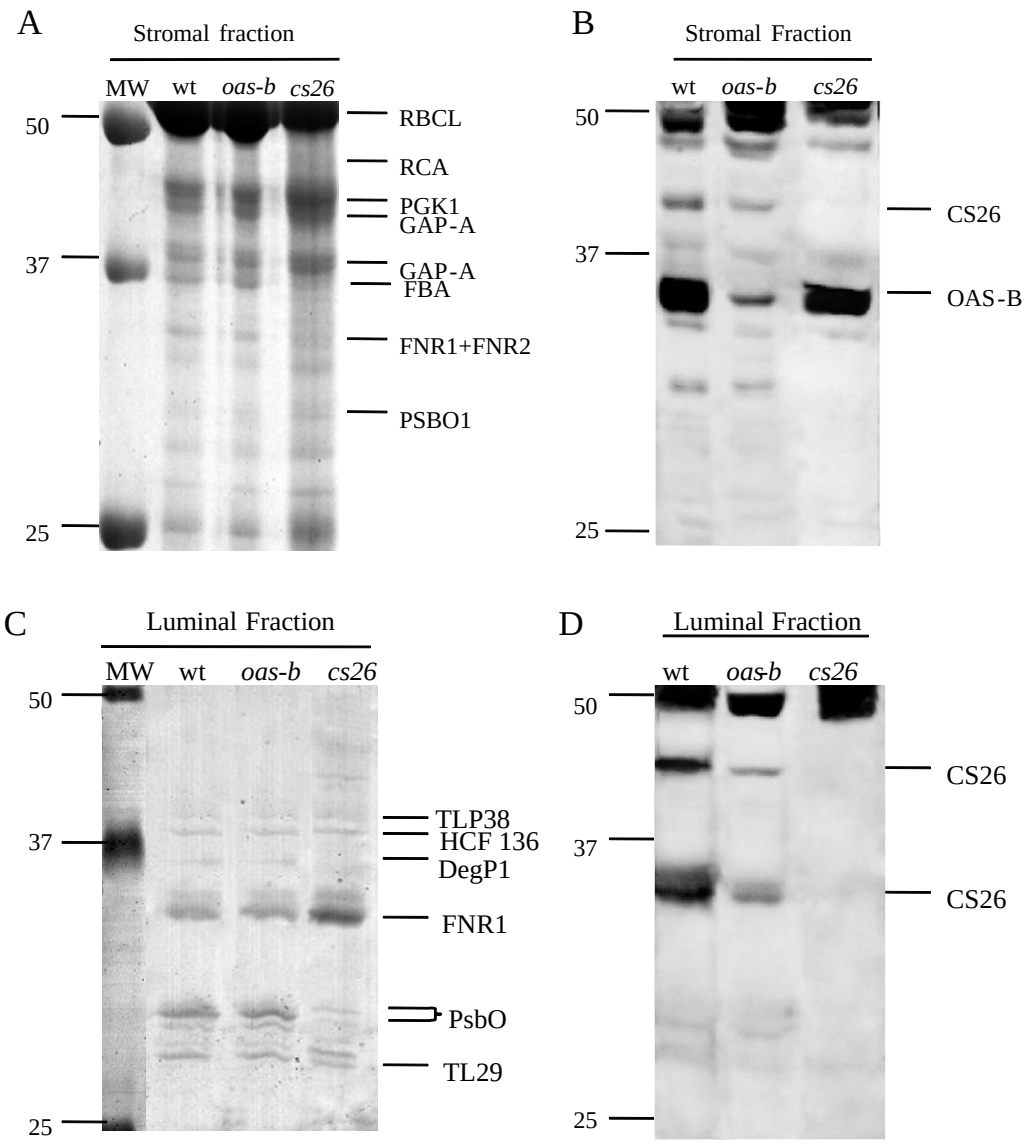

Figure 6. Localisation of CS26 and OAS-B proteins in chloroplast of *Arabidopsis*

Stroma and lumen preparations from *Arabidopsis* were isolated from 40 g of leaves of wild type and *oas-b* and *cs26* mutant plants that were grown for5 weeks under short-day conditions. In all, 100 µg of stromal or 30 µg of lumenal protein extracts was electrophoresed on 12 % acrylamide gels. One replica was stained with Coomassie Blue, A and C, and the second was used for immunoblot analyses using anti-CS26 antibodies, B and D. Proteins identified by MALDI-TOF were: RBCL (Rubisco large subunit), RCA (Rubisco activase), GAP-A (glyceraldehyde 3-phosphate dehydrogenase A subunit), PGK1 (phosphoglycerate kinase 1), FBA (fructose-bisphosphatealdolase, class I), FNR (ferredoxin-NADP(H) oxidoreductase), PsbO (oxygen-evolving enhancer), TL29 (ascorbate peroxidase 4), DegP1 (DEG protease 1), HCF136 (high chlorophyll fluorescence 136), TLP38 (cyclophilin 38). Specific bands for the OAS-B and CS26 proteins that were detected by the antibody are shown. MW: molecular weight markers.

FIGURE 7

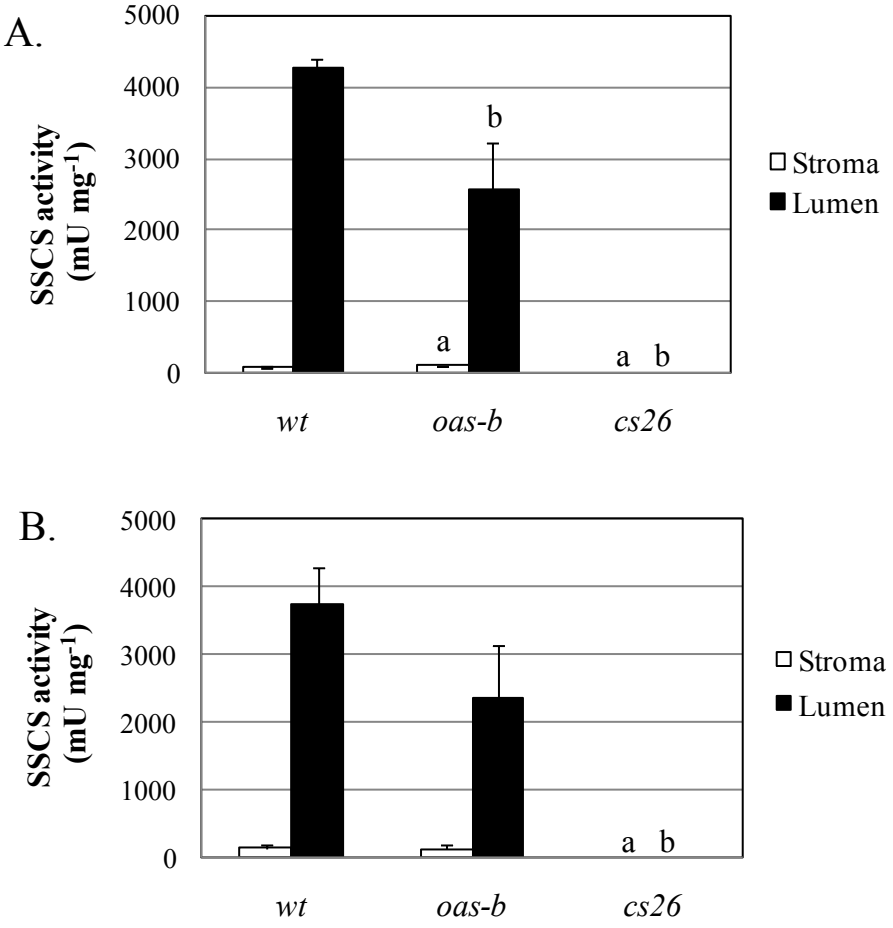

Figure 7. S-sulfocysteine synthase activity in stromal and lumenal fractions under long-day, A, and short-day, B, conditions**.**

SSCS activity was measured in stromal (white columns) and lumenal (black columns) fraction extracts from the chloroplasts of the wild-type and the *oas-b* and *cs26* mutant lines. Values are means ±SD of three independent determinations. Significant differences between mutants and wild type in the stromal fraction are indicated by the letter *a* ($P < 0.05$). Significant differences between mutants and wild type in the lumenal fractions are indicated by the letter *b* ($P < 0.05$).

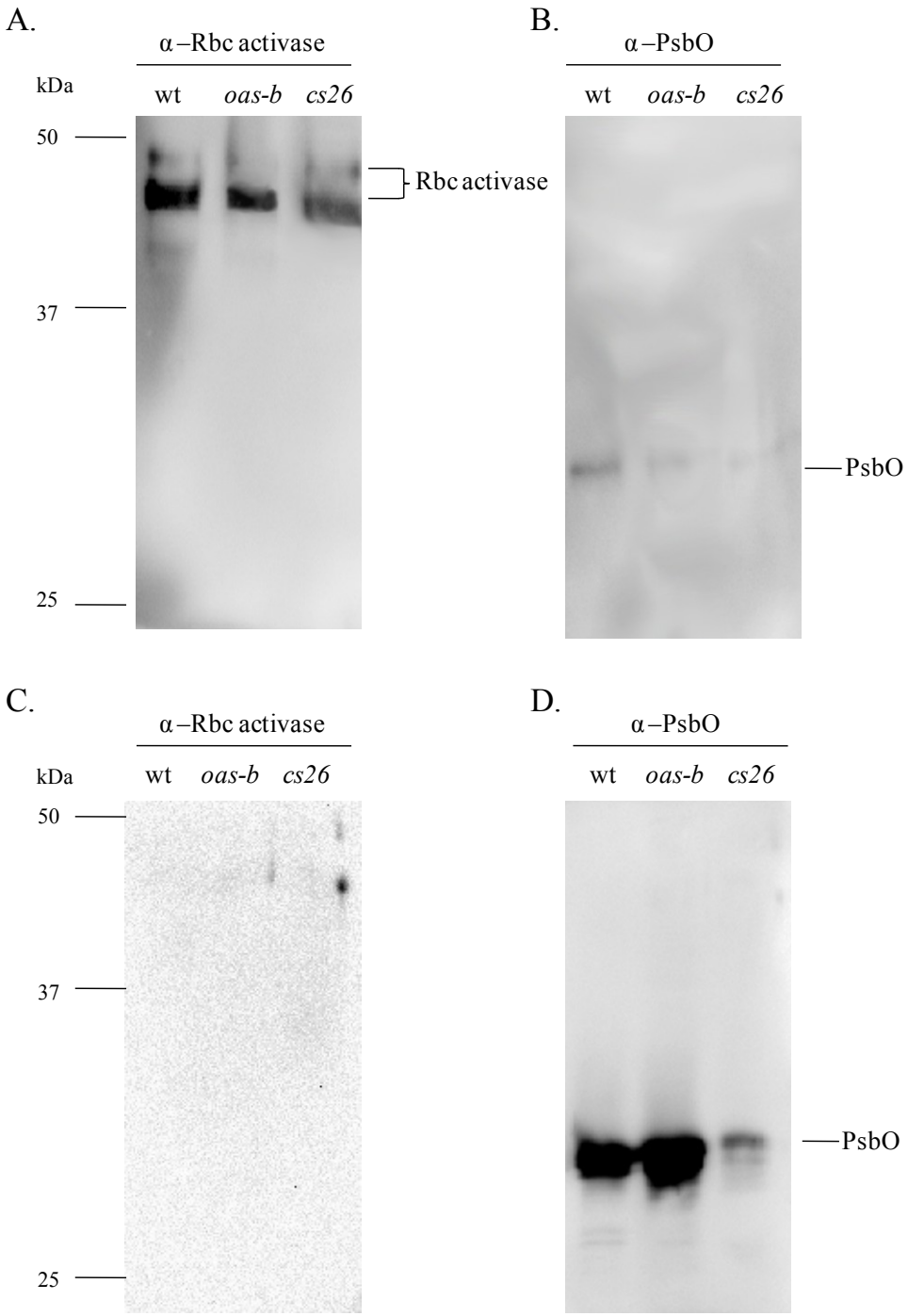

Supplemental Figure S1. Cross-contamination between stromal and lumenal fraction. Stromal and lumenal preparations from *Arabidopsis* were isolated from 40 g of leaves from wild type and *oas-b* and *cs26* mutant plants. To avoid signal saturation of Rubisco activase protein in the stromal extract, only 0.6 µg of stromal protein extracts, A-B, were loaded, and from the lumenal extract, 30 µg of protein, C-D, were loaded. All samples were electrophoresed on 12 % acrylamide gels and used for immunoblot analyses using anti-Rbc activase and anti-PsbO antibodies. A, In the stromal fraction, two bands at 47 and 42 kDa, corresponding with Rubisco activase were observed in all lines with the α-Rbc activase antibody. B, Weak band at 33 kDa corresponding with PsbO was also detected in the stromal extract when α-PsbO was used. There was no signal detection when α-Rbc activase was used in the lumenal extracts.

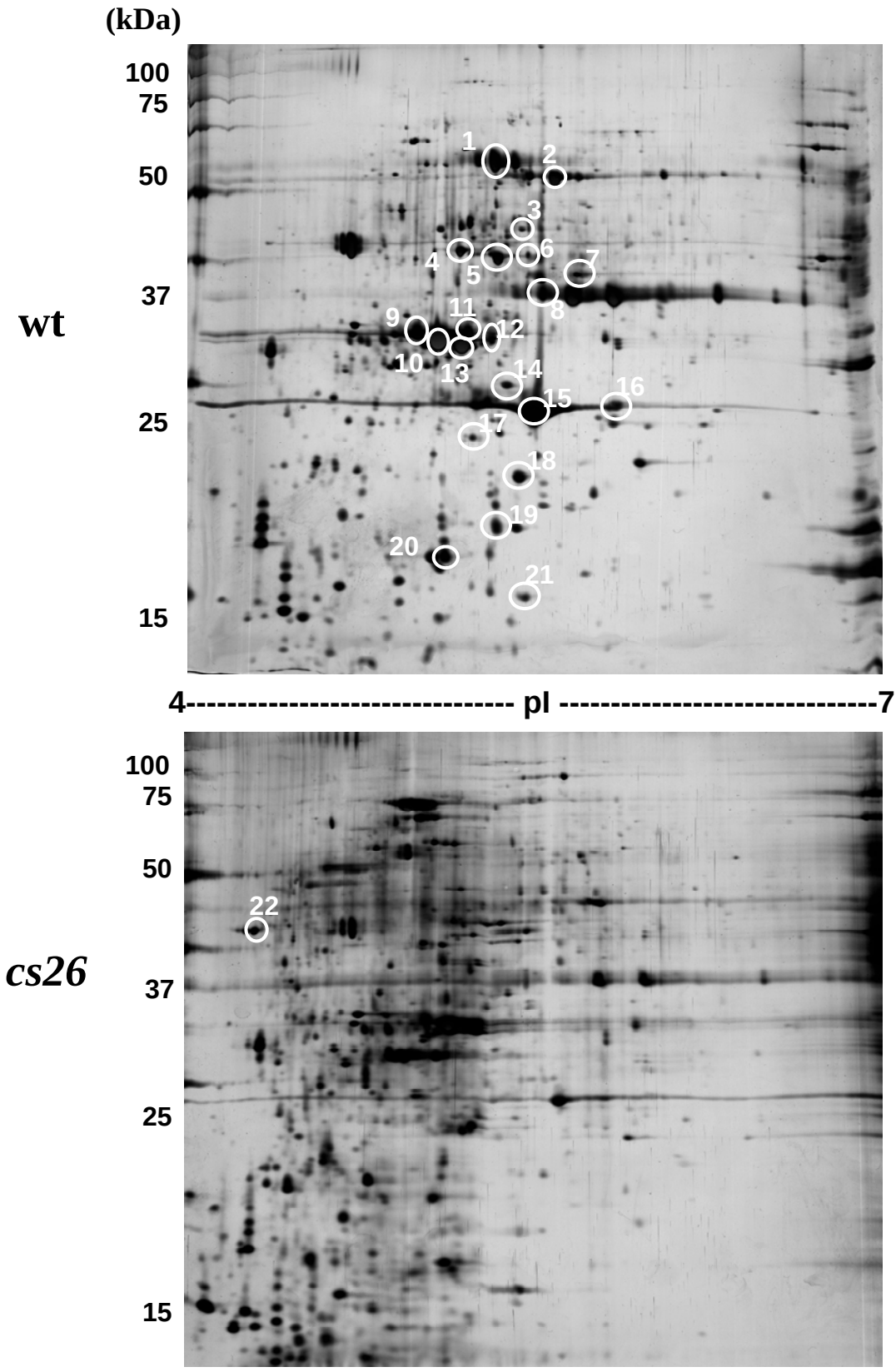

Supplemental Figure 2. Proteome map of the chloroplast lumen of the wild type and mutant *cs26*. It is shown silver-stained two-dimensional gels of 100 mg soluble lumenal proteins from the chloroplasts of 4 week-old plants grown in long-day conditions. The proteins were resolved by SDS electrophoresis in 12% polyacrilamide gel subsequent to isoelectric focusing in a linear immobilized pH gradient from pH 4 to 7. The circles denote protein spot differences that were identified by MALDI-TOF. See Table 6 for detailed information on each identified protein.